

Aus dem Bereich Physiologie
Theoretische Medizin und Biowissenschaften
der Medizinischen Fakultät
der Universität des Saarlandes, Homburg/Saar

Endocytosis of cytotoxic granules in mouse cytotoxic T-lymphocytes on lipid bilayers

**Dissertation zur Erlangung des Grades eines Doktors der Medizin
der Medizinischen Fakultät**

der UNIVERSITÄT DES SAARLANDES

2019

vorgelegt von: Pascal Blatt

geb. am: 28.09.1992 in Quierschied

Ich erkläre hiermit an Eides statt, dass ich die vorliegende Arbeit ohne unzulässige Hilfe Dritter und ohne Benutzung anderer als der angegebenen Hilfsmittel angefertigt habe. Die aus anderen Quellen direkt oder indirekt übernommenen Daten und Konzepte sind unter Angabe der Quelle gekennzeichnet.

Bei der Auswahl und Auswertung folgenden Materials haben mir die nachstehend aufgeführten Personen in der jeweils beschriebenen Weise unentgeltlich geholfen:

1. Frau Dr. Varsha Pattu, Betreuung der Promotionsarbeit.
2. Frau Magarete Klose, Unterstützung bei korrekter Auswahl der Chemikalien und Antikörper in Sektion „Materials and Methods“.

Weitere Personen waren an der inhaltlich-materiellen Erstellung der vorliegenden Arbeit nicht beteiligt. Insbesondere habe ich nicht die entgeltliche Hilfe von Vermittlungs- bzw. Beratungsdiensten (Promotionsberaterinnen/Promotionsberater oder anderer Personen) in Anspruch genommen. Außer den Angegebenen hat niemand von mir unmittelbar oder mittelbar geldwerte Leistungen für Arbeiten erhalten, die im Zusammenhang mit dem Inhalt der vorgelegten Dissertation stehen.

Die Arbeit wurde bisher weder im Inland noch im Ausland in gleicher oder in ähnlicher Form in einem anderen Verfahren zur Erlangung des Doktorgrades einer anderen Prüfungsbehörde vorgelegt.

Ich versichere an Eides statt, dass ich nach bestem Wissen die Wahrheit gesagt und nichts verschwiegen habe.

Die Bedeutung der eidesstattlichen Erklärung und die strafrechtlichen Folgen einer unrichtigen oder unvollständigen eidesstattlichen Erklärung sind mir bekannt.

Homburg, den 10.12.2019

Unterschrift des Promovierenden

1 ABSTRACT

1.1 ENGLISH

Cytotoxic T-lymphocytes (CTLs) are a part of the adaptive immune system. CTLs fight infections by killing bacterially and virally infected target cells as well as tumor cells. They do so by forming a close contact with the infected cells; the contact zone is called immune synapse (IS). It is at the immune synaptic cleft that CTLs release their cytotoxic substances such as perforin and granzymes to kill the infected or tumor cells. Cytotoxic granules (CGs) contain cytotoxic substances and fuse at the IS to release the contents. The fusion of CGs (exocytosis) at the IS, a well-studied phenomenon, is a tightly regulated process. The reuptake of CG membrane components into the CTL after the release of its vesicular contents was shown to be essential for killing of multiple target cells (Chang et al., 2016). CTL-target cell conjugates were used in these confocal fluorescence imaging experiments.

To study this process in more detail regarding spatial and temporal resolution, we used a previously established lipid bilayer system combined with total internal reflection (TIRF) microscopy. The CTLs were isolated from genetically modified synaptobrevin2-mRFP knock-in (Sybki) mice which allowed tracking of the endocytosis of CGs following their exocytosis via the mCherry fluorescence of synaptobrevin2. We used the CG membrane proteins synaptobrevin2 (Syb2) and Lysosomal-associated membrane protein 1 (LAMP1) as a functional readout of endocytosis. We found that Syb2 and LAMP1 both accumulate significantly at the IS following CG exocytosis, whereas Syb2 is exposed to the IS additionally in a CG independent manner after CTL degranulation. We were able to demonstrate that the endocytosis of Syb2 takes place both in a central and peripheral area of the IS. Our results further indicate that the central endocytic events of Syb2 happen within a hotspot, which is located close to the zone of CG exocytosis and at the central supramolecular activation cluster (cSMAC). Finally, the time range of Syb2 endocytosis indicates clathrin-mediated endocytosis as a possible mechanism of CG reuptake.

1.2 DEUTSCH

Zytotoxische T-Zellen (CTLs) sind Teil des adaptiven Immunsystems und verteidigen den Körper gegen bakteriell oder viral infizierte Körperzellen sowie Krebszellen. Dies tun sie, indem sie eine enge Kontaktzone mit ihrer Zielzelle bilden, die sogenannte immunologische Synapse (IS). Innerhalb dieser IS setzen die CTLs zytotoxische Substanzen wie Perforin oder Granzyme frei, um die infizierten oder entarteten Körperzellen abzutöten. Diese zytotoxischen Substanzen sind in zytotoxischen Granula (CGs) gespeichert, die mit der Zellmembran an der IS verschmelzen, um freigesetzt zu werden. Diese Verschmelzung mit der Zellmembran ist ein eng regulierter Prozess, welcher bereits gut erforscht ist. Chang et al. zeigten, dass die Wiederaufnahme der Membranbestandteile der CGs ein wichtiger Mechanismus der CTLs sind, um mehrere Zielzellen hintereinander abtöten zu können (Chang et al., 2016). Für ihre Studie nutzten sie CTL-Zielzellkonjugate und ein konfokales Fluoreszenzmikroskop.

Um diesen Vorgang in größerer zeitlicher und räumlicher Auflösung zu untersuchen, benutzen wir die bereits etablierte Doppellipidschicht in Kombination mit total internal reflection (TIRF) Mikroskopie. Die CTLs wurden von genetisch veränderten synaptobrevin2-mRFP knock-in (Sybki) Mäusen gewonnen, deren CGs fluoreszenzmarkiert sind. Um der Endozytose der CGs nach deren Freisetzung zu folgen, entschieden wir uns, die Membranproteine Synaptobrevin2 (Syb2) und Lysosomal-associated membrane protein 1 (LAMP1) zu verwenden. Wir fanden heraus, dass sich Syb2 und LAMP1 nach der Exozytose der CGs signifikant an der immunologischen Synapse (IS) anreicherten, wobei Syb2 zusätzlich in einer von CGs unabhängigen Weise zur Membran der CTLs transportiert wird. Wir konnten zeigen, dass die Endozytose von Syb2 in der zentralen und peripheren Region der IS stattfindet. Weiterhin lassen unsere Ergebnisse den Schluss zu, dass die Endozytose von Syb2 in der zentralen Region der IS innerhalb eines Hotspots stattfindet, welcher nahe der Zone der CG Exozytose und im central supramolecular activation cluster (cSMAC) liegt. Schließlich liegt die Zeitspanne, in welcher die Endozytose von Syb2 abläuft, im Bereich der clathrin-vermittelten Endozytose, was diese als Mechanismus nahelegt.

2 CONTENTS

1	Abstract	3
1.1	English.....	3
1.2	Deutsch.....	4
3	Abbreviations	7
4	Introduction	8
4.1	Innate and adaptive immunity	8
4.2	T- cell maturation and activation.....	8
4.3	The immunological synapse	10
4.4	MUNC13-4 and its role in CG exocytosis	13
4.5	Endocytosis of CGs	14
4.6	Endocytosis of cytotoxic granules in cytotoxic t-lymphocytes	15
4.7	Lipid bilayer system	16
4.8	Total Internal Fluorescence Microscopy	17
5	Aims of the study	18
6	Materials and Methods	19
6.1	Chemicals, antibodies and buffers.....	19
6.2	Mice and cell culture	22
6.3	Activation of CTLs.....	23
6.4	Lipid bilayer	23
6.4.1	Preparation of proteins	23
6.4.2	Preparation of lipids	23
6.4.3	Cleaning of glass slides	24
6.4.4	Coating of lipids and proteins on glass.....	24
6.5	Total internal reflection microscopy	25
6.5.1	Preparation of the cells for recording	25
6.5.2	Recording	25
6.5.3	Equipment	25
6.5.4	Analysis of CG fusion on the lipid bilayer.....	25

7	Results	27
7.1	Exocytosis of Syb2 and LAMP1	27
7.1.1	Syb2 can be used as a marker for CG membrane exocytosis	27
7.1.2	LAMP1 is a marker for CTL degranulation, but is unspecific for CG membrane exocytosis	32
7.1.3	The rates of synaptobrevin2 and LAMP1 accumulation are similar	36
7.2	Endocytosis of synaptobrevin2.....	38
7.2.1	Endocytosis of Syb2 takes place within cSMAC and pSMAC	38
7.2.2	Central endocytic events happen within a hotspot	40
7.2.3	Endocytosis of Syb2 at the cSMAC is located close to area where CG fusion occurs .	43
7.2.4	Syb2 endocytosis occurs in time range of clathrin-mediated endocytosis	44
8	Discussion	45
8.1	Cytotoxic granule endocytosis – the initial situation.....	45
8.2	Syb2 and LAMP1 exocytosis	45
8.2.1	Syb2 as a marker for CG exocytosis	46
8.2.2	LAMP1 as a marker for CG exocytosis.....	48
8.2.3	Kinetic aspects of LAMP1 and Syb2 accumulation after CG fusion	48
8.3	Endocytosis of synaptobrevin2.....	49
8.4	Limitations and outlook.....	52
9	References	56
10	Acknowledgements	61

3 ABBREVIATIONS

APC	antigen-presenting cell
CG	cytotoxic granule
CTL	cytotoxic T-lymphocyte
GZMB	granzyme B
IS	immunological synapse
LAMP1	lysosomal-associated membrane protein 1
MHC	major histocompatibility complex
mRFP	monomeric red fluorescent protein
SMAC	supramolecular activation cluster
SNARE	soluble N-ethylmaleimide-sensitive factor attachment protein (SNAP) receptor
Syb2	synaptobrevin2
Sybki	synaptobrevin2-mRFP knock-in
TIRF(M)	total internal reflection fluorescence (microscopy)
CME	clathrin-mediated endocytosis

4 INTRODUCTION

4.1 INNATE AND ADAPTIVE IMMUNITY

The human body must always defend itself against pathogens to maintain homeostasis. For this purpose, a complex system of lymphoid tissue called the immune system, comprising humoral and cellular components, has evolved (Parkin & Cohen, 2001).

The immune system consists of two distinct parts, the innate and the adaptive immune system, which interact closely with one another. The innate immune system mediates an unspecific, immediate and highly conserved response to a variety of antigens through highly preserved receptors encoded in the germline (Parkin & Cohen, 2001). In contrast, the adaptive immune system is specific, takes several days to activate and provides an appropriate response adapted to the antigen (Flajnik & Kasahara, 2010). Also, it develops a memory after antigen contact for effective immunity (Medzhitov & Janeway Jr., 1997).

Lymphocytes, as part of the cellular adaptive immune system, consist of B- and T-cells. T-cells are further subdivided into CD8⁺ CTLs and CD4⁺ T-helper cells (Iwasaki & Medzhitov, 2015).

T-helper cells manage the activation or inactivation of immune cells such as B-cells or macrophages by physical interaction and via secretion of cytokines. CTLs, on the other hand, are in charge of effector functions: They kill tumorous or infected body cells by either releasing CGs containing perforin and granzymes or by induction of the Fas pathway (Yatim & Lakkis, 2015).

4.2 T-CELL MATURATION AND ACTIVATION

T-cells are derived from hematopoietic stem cells located in the bone marrow and migrate as naïve cells to the thymus, where they undergo several maturation steps (Andersen et al., 2006). During maturation, gene rearrangement to form the unique T-cell receptor (TCR), as well as positive and negative selection processes take place (Klein et al., 2014).

During positive and negative selection, different types of antigen-presenting cells (APCs) such as cortical thymic epithelial cells (cTECs) present peptides on MHC class I or II complexes to naïve T-cells and induce either proliferation or apoptosis, depending on the strength of antigen recognition: Firm binding to self-peptide/MHC complexes will induce apoptosis of the T-cell while weak recognition will not lead to further positive selection or proliferation. Approximately 90% of the T-cells will undergo apoptosis. This process is the primary mechanism of central tolerance to protect the body from autoimmune diseases (Kyewski & Klein, 2006)

Introduction

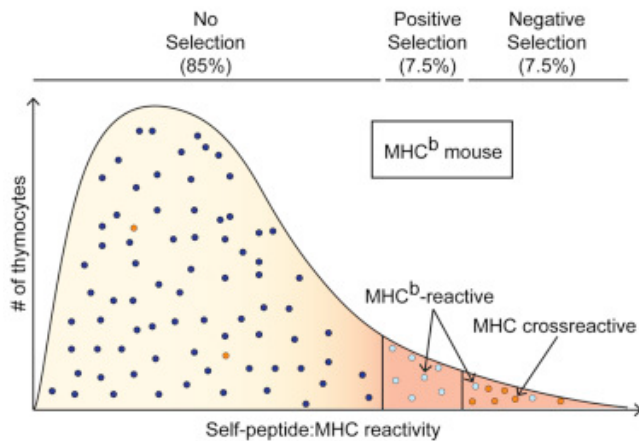


Figure 1. Positive and negative selection of T-cells depends on the strength of self-peptide MHC binding to TCR.

Weak binding of self-peptides results in no further stimulation of growth, strong recognition results in negative selection to avoid auto-immune reactivity. The CTLs which interact with self-peptides neither too weakly nor too vigorously proceed to proliferate. This phenomenon is called positive selection (this figure and legend were taken from McDonald et al., 2015).

Both naïve and mature T-cells then migrate into secondary lymphoid organs such as lymph nodes or spleen, where they make their first antigen contact. The cortex of the lymph node is primarily populated by B-cells whereas T-cells are usually found in the paracortex (Gasteiger et al., 2016). T-cells require antigen-presenting cells (APCs) for activation. Recent data suggest that T-cells randomly travel through the paracortex of the lymph node to encounter their cognate antigen rather than being attracted by the APC (Bogle & Dunbar, 2010).

APCs recognize antigens bound to the major histocompatibility complex (MHC) by the TCR of the T-cell (Weissler & Caton, 2014). Additional costimulatory molecules are necessary to avoid T-cell anergy: The most potent costimulatory molecule is CD28, which interacts with CD80 or CD86 on the APC's membrane resulting in proliferation and production of cytokines (Smith-Garvin et al., 2009).

One major signaling pathway after CD28 co-stimulation is the activation of the phosphoinositide 3-kinase (PI3K). Its activation leads to phosphorylation of phosphatidylinositol (4,5) bisphosphate (PIP₂), converting it to phosphatidylinositol (3,4,5) trisphosphate (PIP₃) localized at the plasma membrane. The Pleckstrin homology (PH) domain of 3-phosphoinositide-dependent protein kinase 1 (PDK1) can then bind PIP₃ and Akt (Boomer & Green, 2010).

The serine/threonine kinase Akt can phosphorylate numerous proteins leading to cell proliferation, migration, and cell survival. Among these proteins are the transcription factors NF- κ B or NFAT regulating the transcription of Interleukin-2 (IL-2) (Huang et al., 2008).

The IL-2 receptor (IL2R) is built of 3 subunits: The constitutively expressed β - and γ -subunits and an α -subunit, which is present on activated T-cells only. The $\beta\gamma$ -IL2R has a moderate affinity to its binding partner, whereas the $\alpha\beta\gamma$ -IL2R interacts firmly with IL-2 (Cornish et al., 2006).

IL-2 is an important growth factor in lymphocytes that activates the transcription factor STAT5, which controls proliferation, apoptosis, differentiation, and inflammation (Rani & Murphy, 2016). In spite of this, the lack of IL2R leads to autoinflammatory diseases in mice. This apparent contradiction may be due to the role of IL-2 in activation-induced cell death (AICD): Lenardo showed that IL-2 upregulates the apoptosis-inducing Fas ligand and TNFR *in vitro* (Lenardo, 1991). Therefore, a lack of IL2R can lead to increased T-cell activation and autoimmune reactions. The significance of this mechanism *in vivo* is unclear, which indicates the complexity of IL-2 effects (Nelson, 2004).

4.3 THE IMMUNOLOGICAL SYNAPSE

The interface between T-cells and APCs or target cells is referred to as the immune synapse (IS) because of several hallmarks which it shares with neuronal synapses: IS formation is a spatially and temporally controlled process, and the IS can be highly dynamic or stable. Furthermore, the IS is a junction at which signals are exchanged, similar to neuronal synapses (Dustin & Colman, 2002).

The IS is organized into concentric rings, which are called supramolecular activation complexes (SMACs). The TCR interacting with its cognate antigenic peptide bound to the MHC complex forms the inner central SMAC (cSMAC). The peripheral SMAC (pSMAC), a ring-like structure of LFA1 attached to ICAM1 on the target cell/APC, surrounds the cSMAC. The pSMAC is acting as a seal for directed killing in the case of CD8⁺ T-cells and is mainly responsible for the stability of the IS (Griffith, 2012). A lateral ring including tyrosine phosphatase CD45 and actin filaments forms the distal SMAC (dSMAC) (Johnson et al., 2000).

A microtubular network assembling during IS formation is responsible for the transport of CGs to the IS in CD8⁺ T-cells. They are probably released in a distinct area of the cSMAC and reach the target cell by diffusion (Stinchcombe et al., 2001). Genetic defects causing impaired CG release in CTLs result in potentially deadly illnesses like Griscelli syndrome 2, hemophagocytic lymphohistiocytosis or Chediak–Higashi syndrome (Chang et al., 2017).

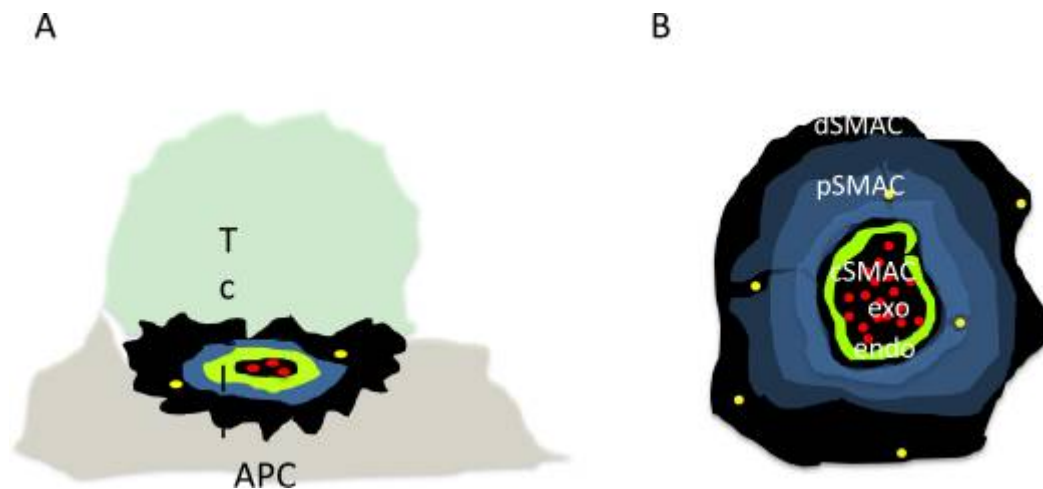


Figure 2. Composition of the IS in an elevated view (A) and Z-section (B).

cSMAC with TCR-peptide/MHC complex interaction and secretory domain, pSMAC including LFA1-ICAM1 bonds and dSMAC as lateral demarcation (this figure and legend were taken from Dustin, 2015).

CGs are the organelles of CTLs and NK-cells responsible for the killing of recognized target cells. They contain granzyme B (GRZMB) and perforin which induce target cell death. CGs are considered to be lysosome-related organelles since they carry the lysosomal markers LAMP1, LAMP-2, and CD63 on their membrane and have an acidic pH, a feature of lysosomes, but also contain perforin and GRZMB (Smyth et al., 2001).

In CTLs, the maturation of CGs starts at the rough endoplasmic reticulum (ER), where the mRNAs of perforin and GRZMB are translated into proteins. Granzymes are bound to M6PR for sorting to early endosomes (EE). Other lysosomal proteins, such as LAMP1, are recruited from the cell membrane. The presence of Rab5, as well as a tubular structure, characterize the EE (Chang et al., 2017). Late endosomes (LEs) budding off from EE carry Rab7 on their cell membrane and have an acidic pH, which leads to dissociation of M6PR from GRZMB and subsequent recycling to the ER (De Saint Basile et al., 2015).

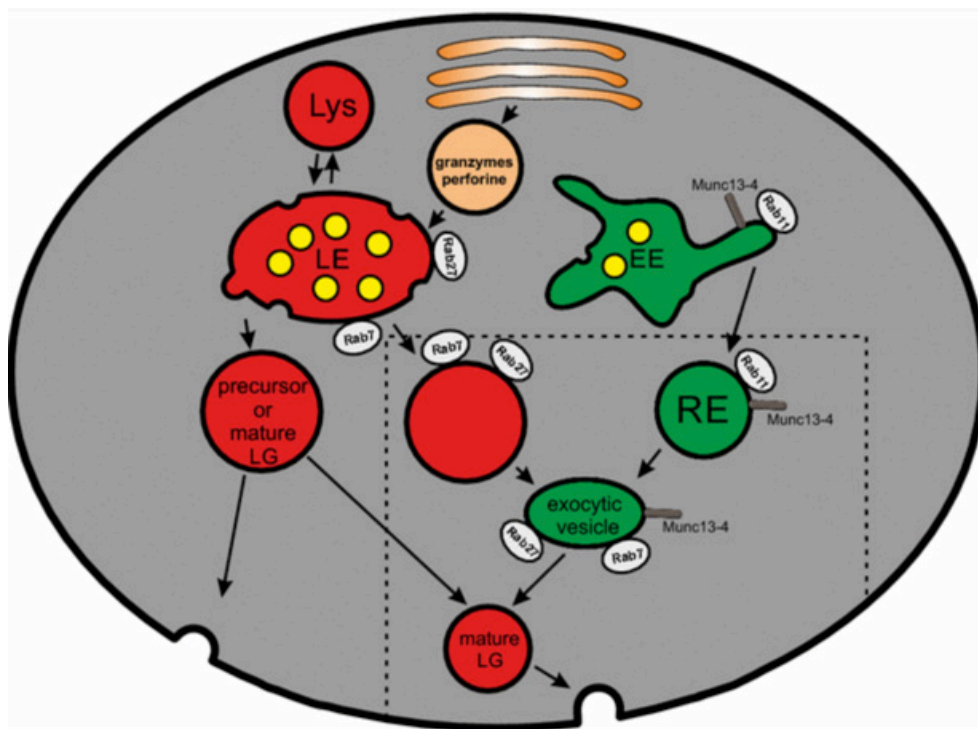


Figure 3. Maturation of CGs.

The maturation of CGs starts with mRNA translation at the ER of perforin and GRZMB and subsequent translocation to LEs which are characterized by Rab7. They release precursor CGs which mature and fuse with the plasma membrane. The dashed box contains a new model introducing a second pathway via REs (this figure and legend were taken from Chang et al., 2017).

SNARE (soluble N-ethylmaleimide-sensitive-factor attachment receptor) complexes are the protein machinery responsible for the fusion of membranes. In CGs, they consist of v (vesicle) -SNARE proteins on the granule membrane and t (target)-SNARE proteins located on the plasma membrane. The vesicles first dock to the cell membrane and are then “primed” to fusion competence. SNARE proteins pull the vesicles and the cell membrane together jointly, leading to the displacement of intracellular water between the layers and allowing their contact. As the membranes are both lipophilic, they can subsequently fuse in an exergonic manner (Ma et al., 2015).

In the case of primary murine CTLs, the dominant v-SNARE protein is Syb2 (Matti et al., 2013). The corresponding v-SNAREs are syntaxin11 and SNAP23 which are delivered to the IS by recycling endosomes. MUNC13-4, which acts as a priming factor, is also required for the exocytosis of CGs (Feldmann et al., 2003).

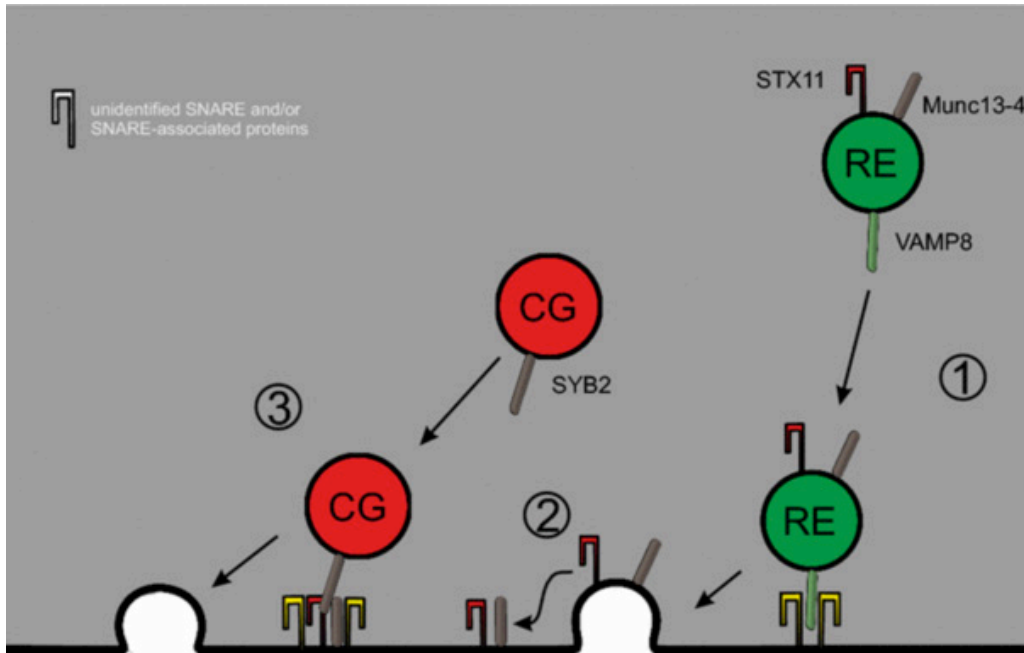


Figure 4. Exocytosis of CGs in CTLs.

(1) RE transport proteins needed for fusion to the IS, such as the t-SNARE syntaxin11 and MUNC13-4. (2) Attachment of those proteins to the cell membrane. (3) The v-SNARE Syb2 on CGs interacts with t-SNARES to release the CGs content (this figure and legend were taken from Chang et al., 2017).

4.4 MUNC13-4 AND ITS ROLE IN CG EXOCYTOSIS

The SNARE associated protein MUNC13-4 acts as a calcium-sensing protein and tightly regulates the fusion process of CGs. In this process, MUNC13-4 is involved in the priming of CG vesicles (Boswell et al., 2012). In MUNC13-4 deficient CTLs, CGs dock frequently but priming and subsequent fusion are drastically reduced (Feldmann et al., 2003).

4.5 ENDOCYTOSIS OF CGs

Endocytosis can generally be subdivided into clathrin-mediated (CME) and clathrin-independent (CIE) endocytosis. CME can either be constitutive or can be ligand-induced. CIE can be dynamin-dependent or dynamin-independent (Mettlen et al., 2010) (Le Roy & Wrana, 2005). Clathrin and dynamin mediate endocytosis of receptor proteins. CME consists of five consecutive steps.

- Nucleation: Accumulation of FCHo proteins leads to the recruitment of epidermal growth factor receptor substrate 15 (EPS15) and intersectins, which in turn leads to AP-2 activation (Henne et al., 2010). Additionally, the F-BAR domain of FCHo proteins seems to form the first budding site at which clathrin eventually binds (Wu et al., 2010).
- Recognition of cargo by specific AP2 domains: AP2 consists of a small (σ), a medium (μ 2) and two large (α and β 2) subunits (Mardones et al., 2013). The μ 2 and σ subunits bind to tyrosine-based motifs on the cargo which are mainly membrane proteins (Rapoport et al., 1998).
- Binding of clathrin to the pit: Soluble clathrin components bind to the β 2 subunit of AP2 leading to conformational changes in the structure of clathrin, which then forms a scaffold around the cavity of the nascent vesicle [referred to as clathrin-coated pits (CCP)] (Owen et al., 2000).
- Scission and un-coating of the vesicle: After invagination mediated by clathrin, the vesicle is still bound to the plasma membrane. Dynamin, a large GTPase, attaches by its BAR domains and polymerizes around the site of vesicle detachment and then mediates the pinching off of the vesicle.

CME is constitutive or ligand-induced. During constitutive CME, non-signaling receptors such as transferrin-R bind to substrates and are then internalized and sorted to lysosomes or recycled back to the cell surface (Watts, 1985). Ligand-induced CME begins by binding of a substrate to a signaling receptor, such as the epidermal growth factor receptor (EGFR). This binding results in endocytosis of receptors, which serves to modulate the strength of a signaling cascade and to adapt the cell response (Beguinot et al., 1984).

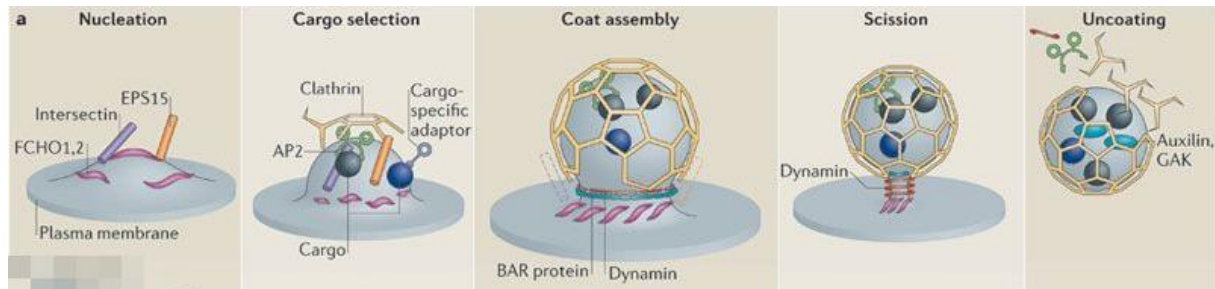


Figure 5. Five-step model of CME.

Nucleation: FCHO proteins recruit intersectins and EPS15 which lead to AP2 clustering. Cargo selection: AP2 assembles various receptors by its μ -subunit and σ -subunit. Coat assembly: clathrin triskelion polymerize and form the clathrin-coated pit (CCP). Scission: GTPase dynamin leads to the scission of the vesicle neck after GTP cleavage. Uncoating: Auxilin or GAK assemble heat shock cognate 70 (HSP70) to cleave the clathrin coat (this figure and legend were taken from McMahon & Boucrot, 2011).

4.6 ENDOCYTOSIS OF CYTOTOXIC GRANULES IN CYTOTOXIC T-LYMPHOCYTES

Chang et al. showed that endocytosis of CGs is clathrin and dynamin-dependent. Endocytosis of CGs is essential for serial killing of target cells as blocking of dynamin-dependent endocytosis results in a 50% reduction of target cell lysis (Chang et al., 2017). It has been demonstrated that the membrane proteins Syb2 and LAMP1 are both endocytosed upon CG fusion, but only Syb2 can be used as a highly specific marker of CG endocytosis (Chang et al., 2017).

4.7 LIPID BILAYER SYSTEM

Until now, anti-CD3 molecules coated on glass coverslips simulated T-cell to target cell interactions in our laboratory. This approach provides the T-cell membrane with limited flexibility and prevents the invagination of the CTL membrane. We cannot use this approach to study the endocytosis of CGs, as this process relies on membrane invagination. The lipid bilayer system has been introduced as a more physiological alternative to overcome those limitations and to study CG endocytosis live *in vitro*.

The lipid bilayer system is composed of three lipids coated on a glass coverslip: A mixture of Capbio, NTA nickel salt, and DOPC serve as a primary lipid. Streptavidin molecules bound to anti-CD3 antibodies are attached to the Capbio macromolecule using streptavidin-biotin bonds. His-tagged ICAM1 proteins are added and form complex formations with the NTA lipid; nickel cations mediate those complex bonds. Kaizuka et al. reported that TCR activation (by anti-CD3 antibodies) and the creation of a pSMAC (by ICAM1-LFA1 interaction) are sufficient to activate a CTL for killing (Kaizuka et al., 2007).

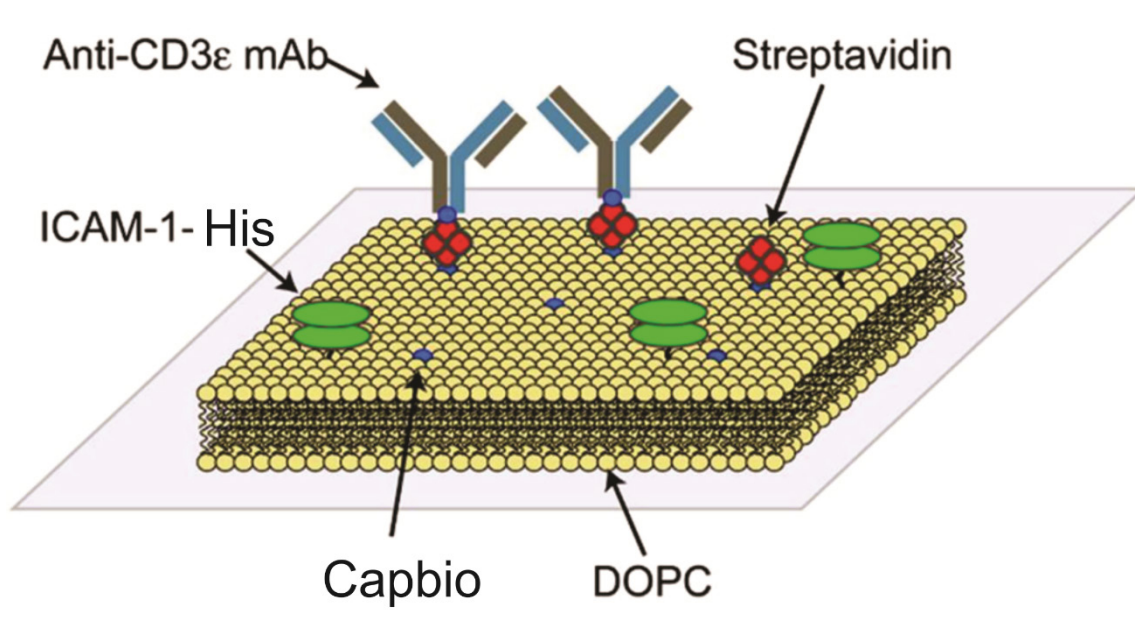


Figure 6. Depiction of the lipid bilayer system.

The primary lipid consists of DOPC macromolecules in which capbio and NTA lipids are integrated. Capbio binds to streptavidin-tagged anti-CD3 antibodies, and the NTA molecules form complex bonds to His-tagged ICAM1 proteins coupled to fluorophore Alexa-405 (this figure and legend were taken from Kaizuka et al., 2007).

4.8 TOTAL INTERNAL FLUORESCENCE MICROSCOPY

In our experiments, we use genetically engineered mice whose v-SNARE synaptobrevin2 is coupled to a fluorophore (synaptobrevin2-mRFP knock-in, Sybki). Using Sybki mice, we can detect CGs *in vitro* using total internal fluorescence microscopy (TIRFM) as it was shown that synaptobrevin2 is primarily located on CGs in mouse CTLs (Matti et al., 2013). The fusion of CGs results in a rapid loss of mRFP fluorescence.

According to Snell's law, light reflects at a vertical reference by passing from a medium with a higher refraction index to a medium with a lower refraction index. The extent of reflection depends on the difference between the refraction indices of the media and the angle in which it reaches the border of the media. Above a particular angle called the critical angle, incident light reflects totally. Some of the reflected light can penetrate across the interface and generates an electromagnetic field. This field is called the evanescent field in the second medium adjacent to the interface, and is capable of illuminating a thin layer (~200 nm) in the second medium; therefore this mode of imaging has a high z resolution and is also called evanescent wave imaging. The resulting background fluorescence is roughly one/2000th of that of epifluorescence microscopy (Pattu et al., 2013).

5 AIMS OF THE STUDY

We want to analyze the spatial and temporal dynamics of CG exo- and endocytosis. We aim to visualize CG endocytosis using the two different CG membrane proteins Syb2 and LAMP1 at a high spatial and temporal resolution. Thus, we would like to enhance our knowledge about the timing and location of the CG membrane endocytosis following exocytosis. By using the advantage of high z-resolution, which TIRFM provides, we want to gather precise information about the position and timing of this reuptake. The lipid bilayer system mimicks the target cell membrane in a highly controlled environment in which we could define lipids and proteins; it also offers the advantage of a more physiological setting than anti-CD3 antibody coated glass coverslips.

6 MATERIALS AND METHODS

6.1 CHEMICALS, ANTIBODIES AND BUFFERS

Chemicals

Human serum albumin (HSA)	Life technologies
Ethylendiaminetriacetat (EDTA)	Sigma-Aldrich
H ₂ O ₂	Sigma-Aldrich
4-(2-hydroxyethyl)-1-piperazineethanesulfonic acid (HEPES)	Merck
Phosphate buffered saline (PBS)	Gibco by life technologies
Roswell Park Memorial Institute (RPMI) medium	Life technologies
Sulfuric acid	Sigma-Aldrich
Trypanblue	Merck
Casein	Sigma-Aldrich
Poly-L-Ornithine	Sigma-Aldrich
IL-2 mouse recombinant protein	Fisher scientific

Lipids

18:1 DGS-NTA 1,2-dioleoyl- <i>sn</i> -glycero-3-[(N-(5-amino-1-carboxypentyl) iminodiacetic acid) succinyl] (nickel salt)	Avanti
18:1 DOPC 1,2-dioleoyl- <i>sn</i> -glycero-3-phosphocholine	Avanti
16:0 Biotinyl Cap PE (capbio) 1,2-dipalmitoyl- <i>sn</i> -glycero-3-phosphoethanolamine-N- (cap biotinyl) (sodium salt)	Avanti

Antibodies

CD3e hamster anti-mouse (clone 145-2C11)	BD Biosciences
CD107a (LAMP1) Monoclonal Antibody (eBioH4A3), Alexa Fluor 488	BioLegend
Anti-RFP antibody	Genway

Materials and Methods

Buffer

0 mM calcium buffer

NaCl	155 mM
KCl	4.5 mM
Hepes	5 mM
MgCl ₂ x 6H ₂ O	3 mM
Glucose	10 mM
Osmolarity	300 ± 10% mOsm
pH	7.3

10 mM calcium buffer

NaCl	140 mM
KCl	4.5 mM
Hepes	5 mM
MgCl ₂ x 6H ₂ O	2 mM
CaCl ₂ x 6H ₂ O	10 mM
Glucose	10 mM
Osmolarity	300 ± 10% mOsm
pH	7.3

Erythrolysis buffer

NH ₄ Cl	155 mM
KHCO ₃	10 mM
EDTA	0.13 mM

Buffer 1

Roswell Park Memorial Institute medium (RPMI)	1 l
FCS	100 ml
Hepes	11 ml 1M
Penicillin/Streptomycin	11 ml

Materials and Methods

Buffer 2

Isolation buffer	500 ml
BSA	1 g
EDTA	4 ml 0.5 M

Buffer 3

AIM V medium	50 ml
beta-mercaptoethanol 40mM	62.5 μ l

HHSA buffer:

HEPES pH 7.2	20 mM
NaCl	137 mM
KCl	5 mM
Na ₂ HPO ₄	0.7 mM
D-glucose	IM
HSA	25 mM
CaCl ₂	1 mM
MgCl ₂	2 mM

Piranha solution

H ₂ O ₂	30%
Sulfuric acid	70%

Lipid buffer

Tris pH 8	25 mM
NaCl	150 mM

6.2 MICE AND CELL CULTURE

Synaptobrevin2-mRFP knock-in (Sybki) mice were generated as described (Matti et al., 2013). Animal killing was performed according to the Animal Welfare Act (Tierschutzgesetz) (permission no. K110/180-07 by the state of Saarland). Splenocytes were extracted from 15-25 weeks old Sybki mice. The isolation of CTLs was performed as a positive isolation using Dynabeads® FlowComp Mouse CD8⁺ kit (Invitrogen).

The spleen was removed and mashed in a preheated RPMI buffer (37 °C). The suspension was centrifuged for 8 min at 1100 rpm. Erythrolysis buffer was added and after 30 seconds, 9 ml of RPMI was added and the suspension centrifuged for 8 min at 1100 rpm.

The RPMI buffer was replaced by the isolation buffer after erythrocyte lysis and the remaining splenocytes were washed a final time by centrifugation before being used for the positive isolation of CD8⁺ T-cells. The pellet was re-suspended in 500 µl of isolation buffer and incubated with 25 µl of anti-CD8 antibodies for 10 minutes on ice. After adding 6 ml of isolation buffer and spinning down at 1400 rpm for 8 minutes, the pellet was re-suspended in 1 ml isolation buffer. The suspension was incubated with 75 µl of magnetic beads for 15 minutes on a rocker at 4 °C.

After adding 5 ml of isolation buffer, the suspension was placed on a magnet for 3 minutes and the supernatant was removed. The suspension was then incubated with 1 ml of release buffer for 10 min on a rotator. The suspension was then placed on a magnet for 3 min again to remove the magnetic beads which were released from the CTLs. The supernatant was transferred to a new falcon tube and 10 µl of the cell suspension was used for cell density determination [most probably number (MPN) procedure] and the suspension was again washed by centrifugation at 1400 rpm for 8 minutes.

For experiments on cells stimulated for three days, the cells were plated at a density of 1 x 10⁶ cells per ml in IMDM. 2 ml of the cell suspension were placed in one well of a 24-well plate. Cells were incubated at 37 °C and 5 % CO₂ for 3 days. Cells were counted on the second day of culture and stimulation and split because the cell density doubled on that day due to proliferation. Cells were plated at a density of 1 million per ml and supplemented with IL-2.

For experiments on day 10 stimulated cells, the cells were plated after isolation at a density of 1 x 10⁶ cells per ml in AIMV medium and supplemented by 100 U of IL-2 per ml. 1 ml of the cell suspension was added to one well of a 24-well plate. Activator Dynabeads which are anti-CD3/anti-CD28 coated beads were added per well at a ratio of 1:0.8 of cells to beads. From day 3 to day 10, cells were counted every day. Beads were removed and cells were plated at a density of 1 million per well and supplemented with IL-2.

6.3 ACTIVATION OF CTLs

To activate the naïve CTLs *in vitro*, the CD3 molecules of the TCR-CD3 complex and the co-stimulatory molecules CD28 were activated by anti-CD3 and anti-CD28 antibody coated beads (Dynabeads®, life technologies). To generate activated T-cells, 0.8 million beads were added per 1 million cells (ratio beads : T-cells 0.8:1). The cells and beads were incubated for 8-10 days.

6.4 LIPID BILAYER

6.4.1 Preparation of proteins

6.4.1.1 Monobiotinylation of anti-CD3 antibodies

EZ-link sulfo-NHS-LC-LC-Biotin (Life technologies) was diluted in DMSO at a concentration of 200 mg/ml. Next, 0.05 µg/ml biotin was added to the pure anti-CD3 antibody (1 mg/ml) solution. This solution was incubated for 30 minutes at room temperature. To purify the product, a dialysis using a dialysis cassette (Slide-A-Lyzer® Dialysis Cassettes, Thermo scientific) was performed overnight at 4 °C in PBS. The last step was to measure the concentration in an aliquot by photometry.

6.4.1.2 Coupling of dylight-405 to ICAM

Mouse ICAM1 was generated from drosophila S2 cell line expressing ICAM1 (kindly provided by Dr. Michael Dustin). The protein was purified after S2 induction and the purified ICAM1 was then labeled with Dylight-405 NHS-Ester (Thermo scientific). ICAM1 protein (in PBS, 1 mg/ml) was prepared in borate buffer at 0.67 M final concentration. Then 50 µg dylight-405 dye were mixed with ICAM1 protein in borate buffer for 1 hour at RT. Finally, the coupled ICAM1 protein was purified by dialysis overnight.

6.4.2 Preparation of lipids

100% DOPC, 25% NTA and 2% capbio for the working stock were prepared in a lipid buffer bubbled with N₂. The lipids were removed from the stock solution and dissolved in DMSO (Avanti). For preparing 1 ml of the lipid mixture, 250 µl of pure DOPC is needed from stock; 212 µl NTA and 188 µl DOPC were mixed to prepare 25% NTA and 7 µl capbio + 246 µl DOPC were mixed to prepare 2% capbio lipid. The lipids (100% DOPC, 25% NTA and 2% capbio) were then dried by lyophilizer for 2 hours at -40 °C. They were then re-suspended in lipid buffer. At this point, a liposome suspension with inhomogeneous sizes of vesicles was generated. To equal the size of vesicles, the suspension was extruded in a vestin extruder (Lipofast®) 20 times until the lipid suspension became transparent. Transparency indicates the formation of SUVs (single unilamellar vesicles) with a homogenous particle size distribution. The next step was to dilute the lipids to a concentration of 0.4 mM each with DOPC.

6.4.3 Cleaning of glass slides

75 ml of piranha solution was prepared by pouring 50 ml of concentrated sulfuric acid into a beaker; 25 ml of hydrogen peroxide was added.

Glass slides were kept in Piranha solution for 20 minutes and washed with milliQ water for 5 minutes. It was important to take the milliQ out of the tap and not the tank to avoid contamination of the glass surface. Glass was dried completely by suction. Afterwards, organic contaminations were removed by plasma cleaning (normal air inside) for 10 minutes.

6.4.4 Coating of lipids and proteins on glass

The reaction chamber was prepared by sticking the cleaned glass slide on the chamber (Ibidi sticky-slide® VI microscopy chamber). It was important to remove all air bubbles between the glass slide and the chamber. Afterwards, 50 µl of liposome solution was applied to the chamber.

Capbio binds with its biotin group to the streptavidin group of the anti-CD3 antibody (concentrations of lipids according to anti-CD3 concentration see table 1).

Next, 10 µl of NiSO₄ (100µM) in 1000 µl Casein (5%) were applied to each well for 20 minutes.

Subsequently, the ICAM-405 His-tag was diluted 1:2000 (stock 0.55 mg/ml) and 3 µl of this dilution was added to each well. In the last step, the biotinylated anti-CD3 antibodies were applied. After each step, the wells were washed 3 times with 100 µl HBS/HAS buffer.

For imaging, the buffer was removed and 50 µl of day 3 or day 10 activated T-cells suspended in 0 mM calcium buffer were seeded freshly onto one well.

Table 1: Lipid compositions

20 µg/ml anti-CD3 antibody

16:0 Biotinyl Cap PE (capbio)	30 µl of 0.4 mM stock
18:1 DGS-NTA	75 µl of 0.4 mM stock
18:1 DOPC	45 µl of 0.4 mM stock

6.5 TOTAL INTERNAL REFLECTION FLUORESCENCE MICROSCOPY

6.5.1 Preparation of the cells for the recording

For experiments with day 3 cells, the anti-CD3/anti-CD28 magnetic beads were removed from the culture on day 3 after activation. The cells rested for 2 hours and then 500 μ l of cells were taken out and resuspended in 50 μ l of 0 mM calcium buffer, before adding them to one well for the lipid bilayer imaging chamber.

For experiments with day 10 cells, the anti-CD3/anti-CD28 magnetic beads were removed from the culture on day 10 after activation. Cells were also allowed to rest for 2 hours and then 500 μ l of cells were taken out and resuspended in 50 μ l of 0 mM calcium buffer, before adding them to one well of the lipid bilayer.

6.5.2 Recording

The lipid buffer was removed from the well, and then 50 μ l of the cell suspension was added to the well. Cells were visualized by brightfield until they settled and attached (2-3 minutes). 100 μ l of 10 mM calcium solution with anti-LAMP1-488 (0.005 mg/ml) or anti-RFP-488 (\sim 0.01 mg/ml, according to the labeling efficiency) was perfused and dual channel recording of the 488 nm and 561 nm channels (5Hz acquisition frequency) was performed for 20 minutes.

6.5.3 Equipment

The recordings were performed at a total internal reflection microscope (Visitron, Puckheim, Germany) consisting of an inverted Optical IX microscope (Olympus, Hamburg), solid-state lasers (Visitron Systems) having wavelengths of 561 nm, 488 and 405 nm. The TIRF condenser was based on the iLAS² (Roper Scientific, Evry, France) that allows even TIRF illumination and a multiband filter set (AHF, Tübingen, Germany). The camera was a back-illuminated EMCCD Evolve 512 (Photometrics, Tucson, AZ, USA). Acquisition rate was set to 5 Hz and the exposure time to 200 ms. The analysis of the recorded material was performed using imageJ software (National Institutes of Health NIH, ML, USA).

6.5.4 Analysis of CG fusion on the lipid bilayer

Cells were prepared as described above, seeded onto the lipid bilayer and imaged in TIRF mode to visualize CG fusion.

Fusing CGs had to be distinguished from non-fusing and quickly regressing CGs. This was done by analyzing the fluorescence intensity of the particular CG over time.

The images in figure 7A show a frame by frame display of one CG fusion event. Before fusing, the CG arrives at the surface of the coverslip and becomes very bright. This increase in brightness before fusion indicates a tight interaction of the vesicle and the cell membrane and should be seen before every fusion event. The fluorescence intensity then drops within 5 frames or less, when imaged at an acquisition frequency of 10 Hz (varying acquisition frequencies accordingly). In addition, a brief flash

Materials and Methods

upon fusion is observed. The flash indicates the dispersion of the granule membrane-bound Syb2-mRFP over the CTL membrane. The sudden increase in brightness, fast loss of fluorescence intensity and the flash upon fusion distinguishes a fusing CG from a CG rapidly moving back into the cytoplasm. The latter shows no increase in fluorescence intensity before the drop and the drop in intensity takes more than 5 (usually more than 10) frames; in addition, no flash is observed.

The graph in figure 7B shows the fluorescence intensity of a CG over the time frames of the fusion event as visualized by TIRFM. The increase in fluorescence intensity followed by the loss in fluorescence can be clearly used to identify fusion events.

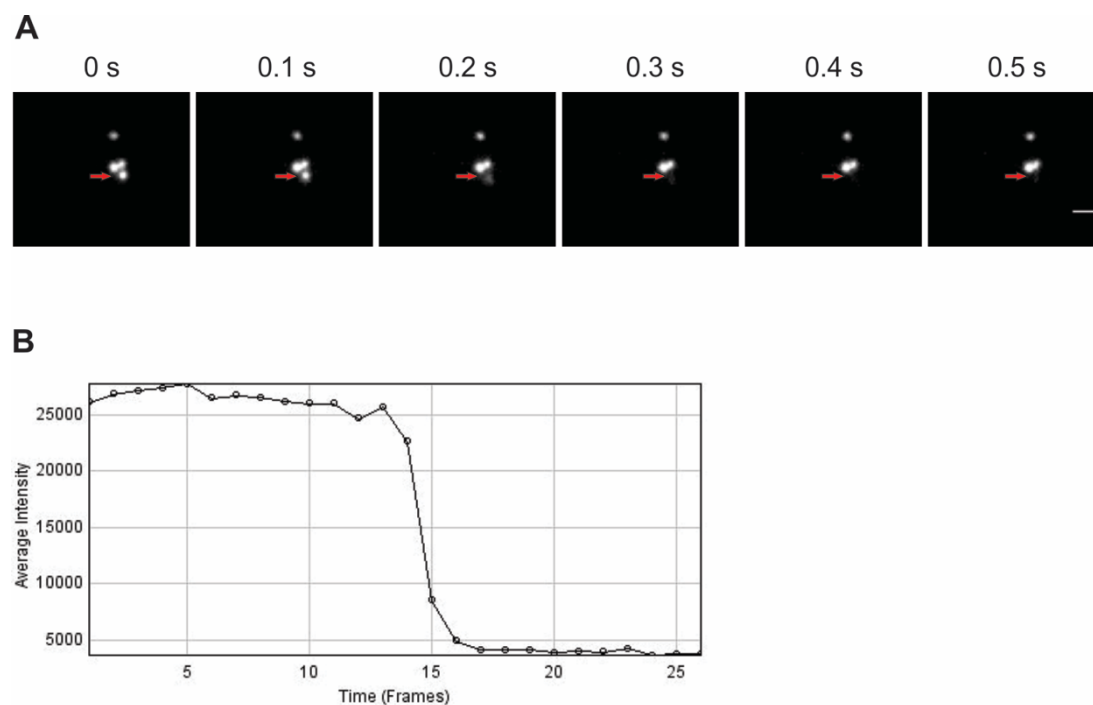


Figure 7. Fusion of CGs by Sybki cells can be clearly identified using TIRF microscopy.

(A) Snapshot images of one CG fusion event from live cell TIRF recording (acquisition frequency 10 Hz). Red arrows point to one fusion event. Scale bar 2 μm . (B) Time trace analysis of the CG fusion event from A showing the changes in fluorescence intensity before and after fusion.

7 RESULTS

To visualize CG endocytosis live in activated CTLs, we chose two CG membrane components for a functional readout. Those proteins are Syb2 and LAMP1. We used CTLs from a Syb2-mRFP knock-in mouse so that we could visualize Syb2 endocytosis after CG fusion by a fluorescently tagged anti-RFP antibody. Since the mRFP tag lies in the lumen of the vesicle, it can only be recognized by the anti-RFP antibody upon CG fusion. This fusion event leads to exposure of the mRFP dye to the extracellular environment. Therefore, unless the cells are permeabilized, the anti-RFP can bind to the mRFP tag on the Syb2-mRFP vesicles only after fusion. Following exocytosis, Syb2-mRFP retention at the plasma membrane or endocytosis can be visualized by the fluorescently labeled anti-RFP antibody.

LAMP1 is known to be a significant component of the CG membrane (Matti et al., 2013). Upon CG fusion, LAMP1 integrates into the plasma membrane before being re-internalized. For this reason, externally applied fluorescent anti-LAMP1 antibodies can bind to LAMP1 on the luminal side of CGs only after CG fusion. After CG fusion, its epitope is exposed extracellularly, and the antibodies gain access to them. Based on the same principle, we used a fluorescently labeled anti-LAMP1 antibody to observe CG membrane endocytosis by TIRFM.

We expected that there would be an increase in the signal from the fluorescent antibodies after fusion. This increase is because more molecules of Syb2 and LAMP1 are present in the CTL membrane. We also expect these proteins to be recycled via endocytosis after CG fusion.

We first compared the anti-LAMP1 and anti-RFP signals in CTLs in which CGs fused and in CTLs in which we did not observe fusion.

7.1 EXOCYTOSIS OF SYB2 AND LAMP1

7.1.1 Syb2 can be used as a marker for CG membrane exocytosis

Cells prepared as described in section 6.5.1 were seeded onto the lipid bilayer system and recorded by TIRFM as described earlier. Figure 8 depicts the fusion of CGs and the subsequent Syb2 accumulation over time. The first image shows the time frame before CG fusion indicated by a flash (Sybki channel, yellow arrow).

Syb2-mRFP accumulated after CG fusion (green). The delay between CG fusion and appearance of Syb2 signal in the anti-RFP channel is likely due to a subthreshold concentration of Syb2 molecules seconds after CG fusion. Later, the anti-RFP particles accumulate further and exceed the detection limit. As expected, there is a co-localization of the endogenous Syb2 signal (Sybki channel) and the anti-RFP signal, indicated by yellow dots in the merged images (yellow arrows at 450 seconds), Pearson coefficient ' r ' of 0.61. This co-localization results from specific binding of the anti-RFP antibodies to the Syb2-mRFP of CGs which also contain LAMP1.

Results

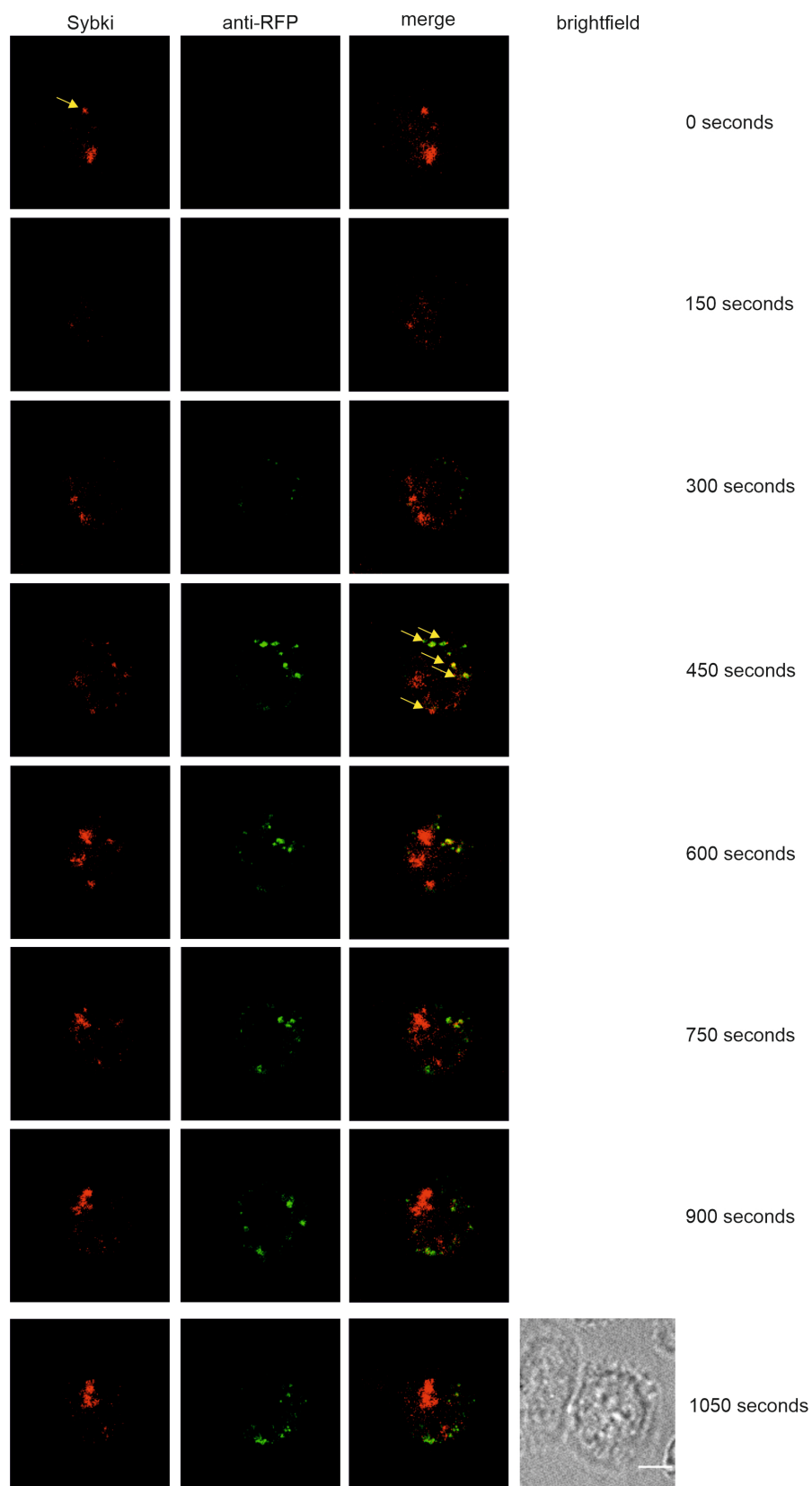


Figure 8. Anti-RFP accumulates after CG fusion and co-localizes with endogenous Syb2 signal.

Yellow arrows at time frame 0 seconds in the Sybki channel indicate a CG that will fuse. The yellow arrows at the time frame 450 seconds in the merged channel highlight anti-RFP and Sybki co-localization. Sybki cells were plated on the lipid bilayer in a 0 mM extracellular calcium solution which was replaced with 10 mM calcium solution containing anti-RFP-488 prior to imaging in TIRF. Cells were excited by the 488 and 561 lasers with an interval of 100 ms to record anti-RFP-488 and Sybki fluorescence, respectively. Acquisition frequency: 5 Hz per channel. Scale bar 5 μm .

Results

Figure 9 shows the fluorescence intensity signal of anti-RFP-488 (indicating Syb2) in cells in which CG fusion occurred (black line) and in cells that did not show CG fusion (red line). Sybki cells were seeded on lipid bilayers and flushed with a 10 mM calcium solution containing anti-RFP antibodies. Cells were then excited by lasers having a wavelength of 488 nm (for anti-RFP-488) and 561 nm (for Sybki) and imaged in TIRF mode for 20 minutes. The fluorescence intensity of anti-RFP-488 in cells that showed CG fusion reached a maximum value of 825 ± 77 arbitrary units, and in cells that did not show CG fusion reached a maximum amount of 424 ± 67 arbitrary units.

Thus, we could demonstrate a significantly higher increase of Syb2-mRFP at the IS of CTLs that showed CG fusion compared to those cells that did not show CG fusion (Mann-Whitney-U test $U = 671367$, $P = <0.001$). We also observed an increase in fluorescence in the TIRF plane in cells that did not fuse CGs.

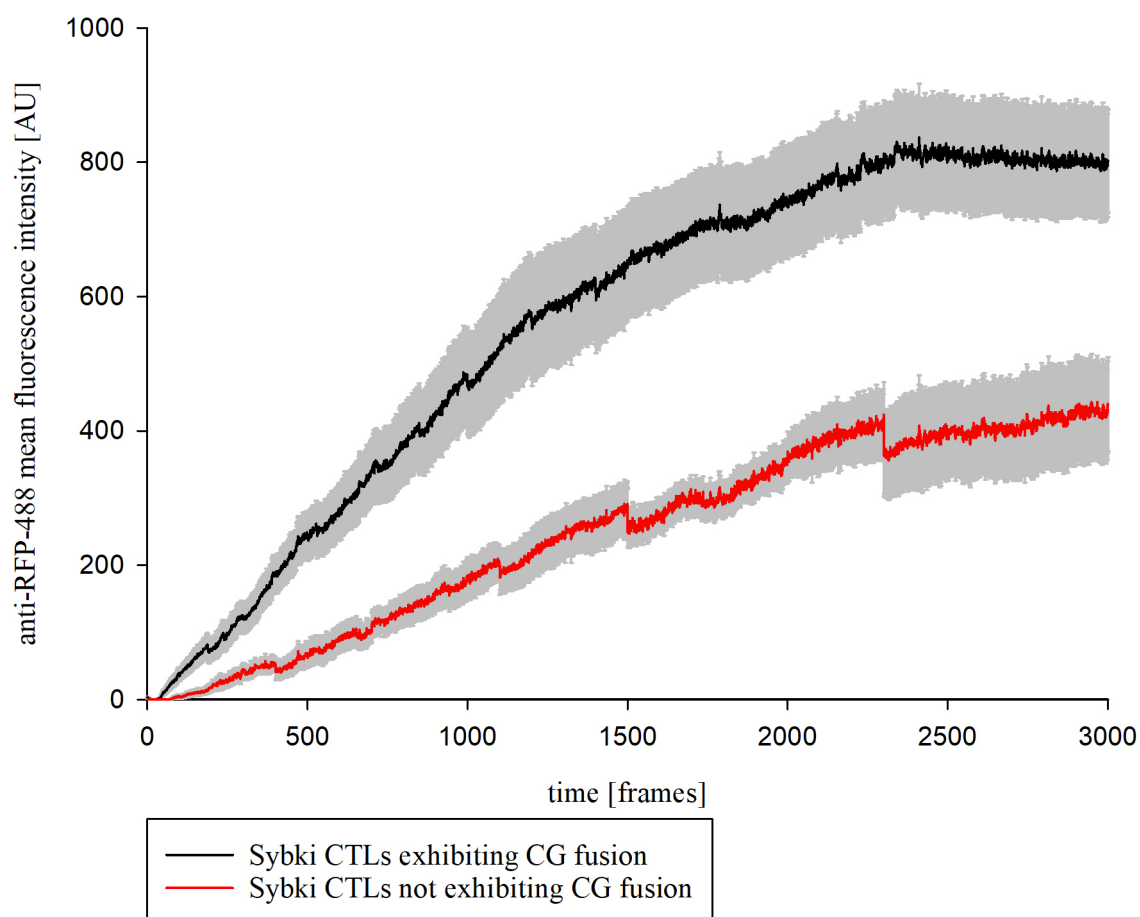


Figure 9. CTLs in which fusion occurs accumulate more Syb2 than CTLs in which fusion does not occur.

There is a significantly higher increase in fluorescence of CTLs that showed CG fusion (black line) in contrast to cells that do not show CG fusion (red line). Error bars represent SEM, Mann-Whitney-U test $U = 671367$, $P = <0.001$. $N=3$, $n=27$ (black line), $n=13$ (red line).

Results

We performed similar experiments on Sybki-MUNC13-4 knock-out mice. As described in section 4.4, in Munc13-4 deficient CTLs, CGs dock but do not fuse. These CTLs are well-suited as a negative control for CG fusion and subsequent anti-RFP accumulation.

Figure 10 shows the fluorescence intensity signal of anti-RFP-488 in CTLs, which showed CG fusion (black line), and Sybki-MUNC 13-4 knock-out CTLs which did not (red line). The fluorescence intensity of anti-RFP-488 in Sybki CTLs that showed CG fusion reached a maximum value of 825 ± 77 arbitrary units, whereas in CTLs from Sybki-MUNC13-4 KO mice it reached a value of 295 ± 30 arbitrary units. Notably, very few fusion events took place in Sybki-MUNC 13-4 knock-out CTLs; those CTLs in which CG fusion occurred yet, were excluded from the analysis.

The Syb2 concentration on plasma membranes of fusing CTLs is significantly higher than in non-fusing CTLs (Mann-Whitney-U test $U = 236664$, $P = <0.001$). This difference indicates that the increase in Syb2 molecules on the plasma membrane occurs mostly upon CG fusion.

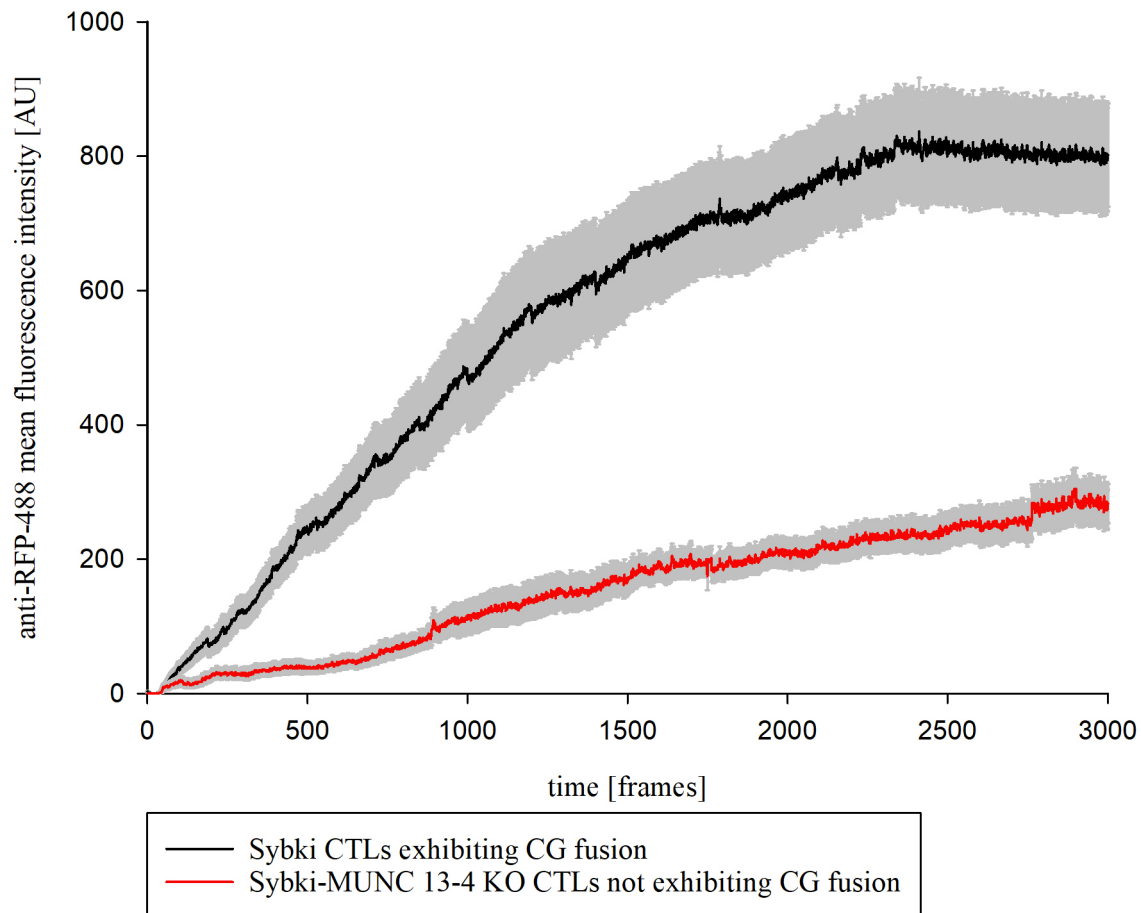


Figure 10. The Syb2 concentration in CTLs that showed CG fusion is much higher than in Sybki-MUNC13-4 KO cells which did not show CG fusion.

There is less anti-mRFP fluorescence in CTLs from Munc13-4 KO mice (red line) than in CTLs from Sybki mice that showed CG fusion (black line). Error bars represent SEM, Mann-Whitney-U test $U = 236664$, $P = <0.001$. $N=3$, $n=27$ (black line), $n=23$ (red line).

From figure 9 and 10, we conclude that the Syb2 concentration at the IS is significantly higher in CTLs in which CG fusion occurs as compared to CTLs in which fusion does not occur (1.94 ± 0.52 ratio in fusing/non-fusing Sybki CTLs and 2.85 ± 0.55 ratio in fusing Sybki and non-fusing Sybki-MUNC13-4 KO CTLs). This indicates that we can use the anti-RFP-488 antibodies to track exo- and subsequent endocytosis with a reasonable specificity for CG membranes. The slight increase of Syb2 in activated but non-fusing CTLs could display a minor occurrence of this protein at the IS independent of CG fusion; this presence of Syb2-mRFP in these cells seems to be stimulus-dependent.

7.1.2 LAMP1 is a marker for CTL degranulation, but is unspecific for CG membrane exocytosis

As an independent marker for CG exocytosis, we intended to use a fluorescently labeled anti-LAMP1-488 antibody. We did so, as it is a widely used degranulation marker for CTLs in FACS (Andrews, 2017). We performed experiments like the ones previously described (section 7.1.1), but replaced the anti-RFP antibody with an anti-LAMP1 antibody. We prepared the cells as described in section 6.5.1 and seeded them onto the lipid bilayer system to record them by TIRFM.

Figure 11 shows CG fusion and LAMP1 accumulation over time. The first image shows the time frame before CG fusion, indicated by a flash [yellow arrow at 0 seconds (Sybki channel)]. A second yellow arrow points towards a second CG, which will fuse (150 seconds, Sybki channel). The delay in time between CG fusion and anti-LAMP1 accumulation is likely due to a concentration of LAMP1 molecules under the detection limit seconds after CG fusion (see also figure 8).

Interestingly, we did observe a weak co-localization between the endogenous Syb2 signal (Sybki signal) and the anti-LAMP1 fluorescence, as indicated by the low amount of yellow dots, Pearson coefficient ' r ' of 0.30. The latter means that LAMP1 is exocytosed upon degranulation by CGs, but the major part of LAMP1 is not derived from CGs making LAMP1 a marker for degranulation but not specific for CG membrane fusion. We conclude that LAMP1 and Syb2 have different paths of exocytosis and, therefore, different paths of endocytosis. In our studies in which we want to follow CG membrane reuptake, LAMP1 is not a suitable marker.

Results

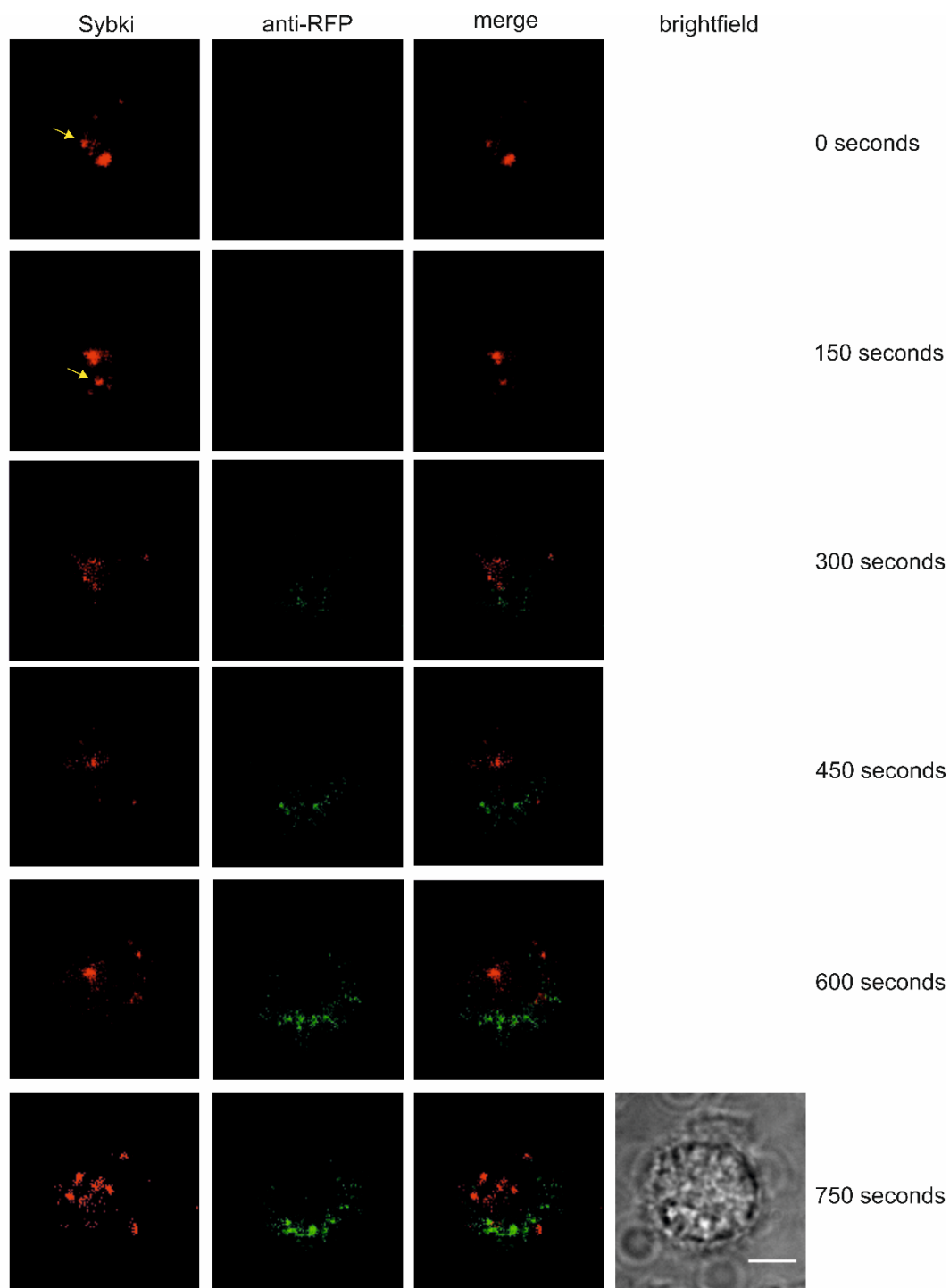


Figure 11. Anti-LAMP1 accumulates after CG fusion and does not co-localize with endogenous Syb2.

The yellow arrows at time frame 0 and 150 seconds in the Sybki channel point towards a CG that will fuse. Sybki cells were plated on the lipid bilayer in a 0 mM extracellular calcium solution and then flushed with a 10 mM calcium buffer containing anti-LAMP1-488 and imaged in TIRF. Cells were excited by the 488 and 561 lasers with an interval of 100 ms to record anti-LAMP1-488 and Sybki fluorescence, respectively. Acquisition frequency: 5 Hz per channel. Scale bar 5 μ m.

Figure 12 shows the fluorescence intensity of anti-LAMP1-488 in cells in which CG fusion occurred (black line) and in cells in which CG fusion did not occur (red line). Sybki cells were seeded on lipid bilayers and flushed with 10 mM calcium buffer containing anti-LAMP1 antibodies. Cells were then

Results

excited by the lasers having a wavelength of 488 nm (for anti-LAMP1-488) and 561 nm (for Sybki) and imaged in TIRF mode for 20 minutes.

The fluorescence intensity of the anti-LAMP1 channel that showed CG fusion has a maximum at 785 ± 62 arbitrary units (black line); in CTLs without CG fusion, the maximum signal is 186 ± 33 arbitrary units (red line).

Thus, there was a significantly higher exposure of LAMP1 to the extracellular space in CTLs that showed CG fusion compared to cells that did not show CG fusion (Mann-Whitney-U test $U = 47702$, $P = <0.001$). The increase of anti-LAMP1 in non-fusing cells compared to fusing cells is lower than the Syb2 increase in non-fusing CTLs compared to fusing cells (0.22 ± 0.07 ratio in the case of LAMP1, 0.51 ± 0.11 ratio in case of Syb2).

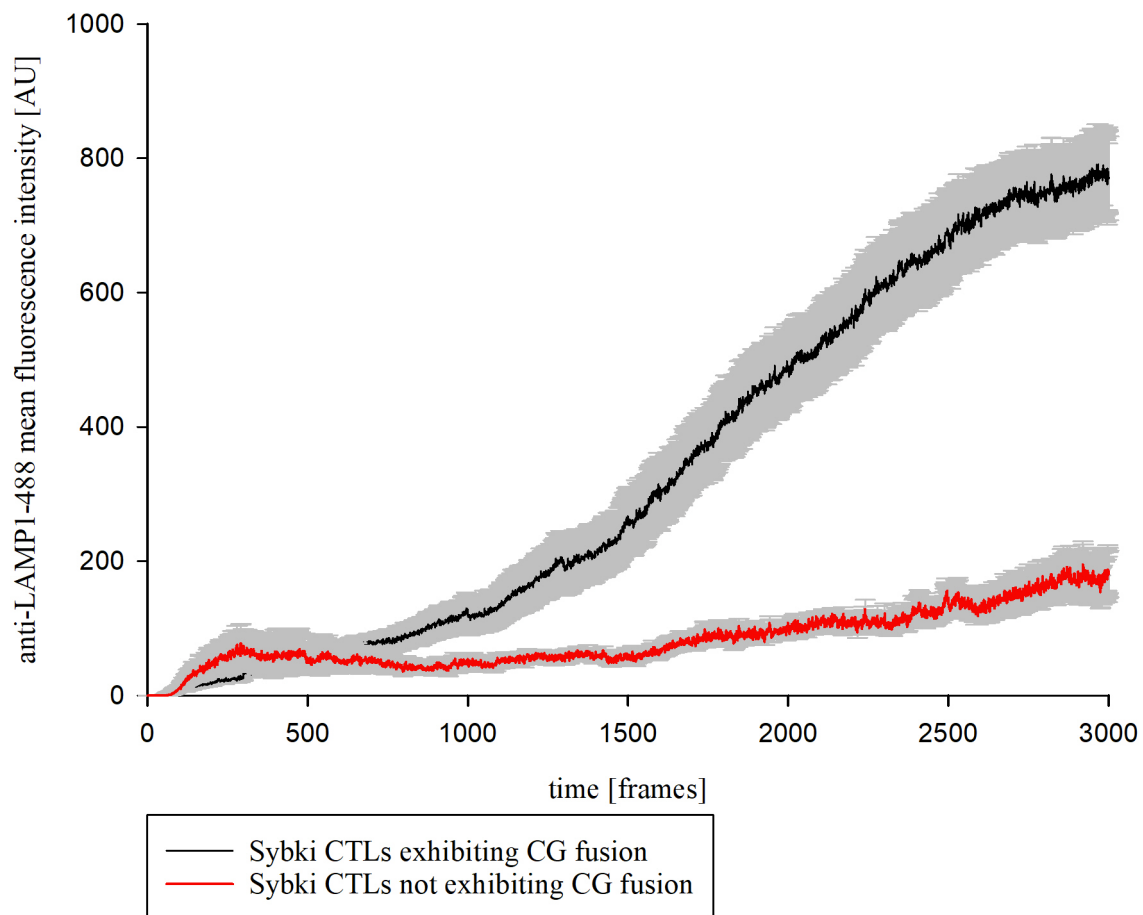


Figure 12. The anti-LAMP1 signal in CTLs which showed CG fusion is significantly higher than the anti-LAMP1 signal in CTLs which did not show CG fusion.

There was a significantly higher increase in fluorescence of CTLs that showed CG fusion (black line) in contrast to cells that did not show CG fusion (red line). Error bars represent SEM, Mann-Whitney-U test $U = 47702$, $P = <0.001$. $N=3$, $n=20$ (black line), $n=9$ (red line).

Results

To confirm the selectivity of this result, we repeated this experiment using Sybki CTLs from MUNC13-4 knock-out mice: In figure 13, the black line indicates the anti-LAMP1 fluorescence intensity of CTLs from Sybki mice in which CGs fused, and the red line indicates the anti-LAMP1 fluorescence of Sybki-MUNC13-4 KO cells in which CG fusion did not occur. The fluorescence intensity of Sybki CTLs that showed CG fusion reached a maximum value of 785 ± 62 arbitrary units, whereas in CTLs from Sybki-MUNC13-4 KO mice, it reached a value of 144 ± 25 AU.

The anti-LAMP1 increase of Sybki-MUNC13-4 KO was again significantly lower than that observed in Sybki cells that showed CG fusion (Mann-Whitney-U test $U = 35466$, $P = <0.001$). The increase in LAMP1 is also lower than the anti-RFP increase in Sybki-MUNC13-4 KO cells (~18 %) compared to Sybki CTLs after CG fusion.

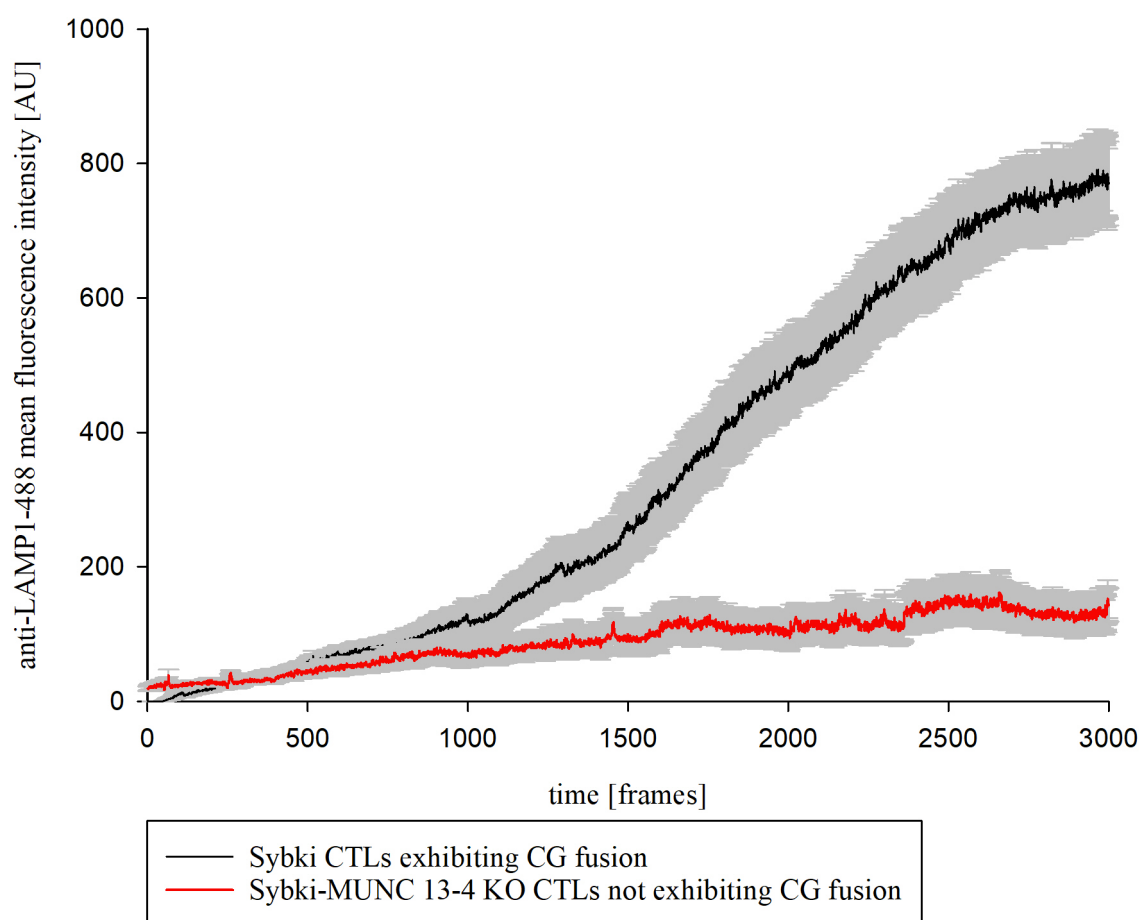


Figure 13. The fluorescence intensity of anti-LAMP1 is significantly higher in Sybki CTLs which showed CG fusion than in Sybki-MUNC13-4- KO CTLs which did not show CG fusion.

There is a significant decrease in anti-LAMP1 fluorescence in CTLs from Sybki-Munc13-4 KO mice that did not show any fusion (red line) in contrast to CTLs from Sybki mice that showed CG fusion (black line). Error bars represent SEM, Mann-Whitney-U test $U = 35466$, $P = <0.001$. $N=3$, $n=20$ (black line), $n=22$ (red line).

Results

From figures 12 and 13, we conclude that the exposure of LAMP1 to the extracellular anti-LAMP1 antibodies is significantly higher after CG fusion (4.4 ± 1.1 ratio in fusing/non-fusing Sybki cells, 5.6 ± 1.4 ratio in fusing Sybki/non-fusing Sybki MUNC13-4 KO CTLs). The anti-LAMP1 accumulation in non-fusing CTLs is negligible, demonstrating that anti-LAMP1 accumulation is a marker for CTL degranulation.

7.1.3 The rates of synaptobrevin2 and LAMP1 accumulation are similar

We analyzed the increase of anti-LAMP1-488 and anti-RFP-488 fluorescence in two different sets of experiments following the first fusion event (figure 14). To compare the two data sets accurately, the fluorescence intensity traces were normalized to the first event of CG fusion in every cell. We demonstrate that the increase in fluorescence of anti-LAMP1-488 and anti-RFP-488 occurs at a similar rate. After 1000 frames, the anti-RFP signal rises from 0 to 537 ± 53 , the anti-LAMP1 signal from 0 to 516 ± 38 arbitrary units. After 2000 frames, the anti-RFP signal accumulates to 729 ± 63 , the anti-LAMP1 signal to 695 ± 44 arbitrary units. A Mann-Whitney-U statistical test was not performed because we used two different fluorophores (anti-RFP-488 and anti-LAMP1-488). We conclude that Syb2 is present on CGs and a specific CG membrane marker as it is exocytosed to the IS following CG fusion together with the well-established degranulation marker LAMP1.

Results

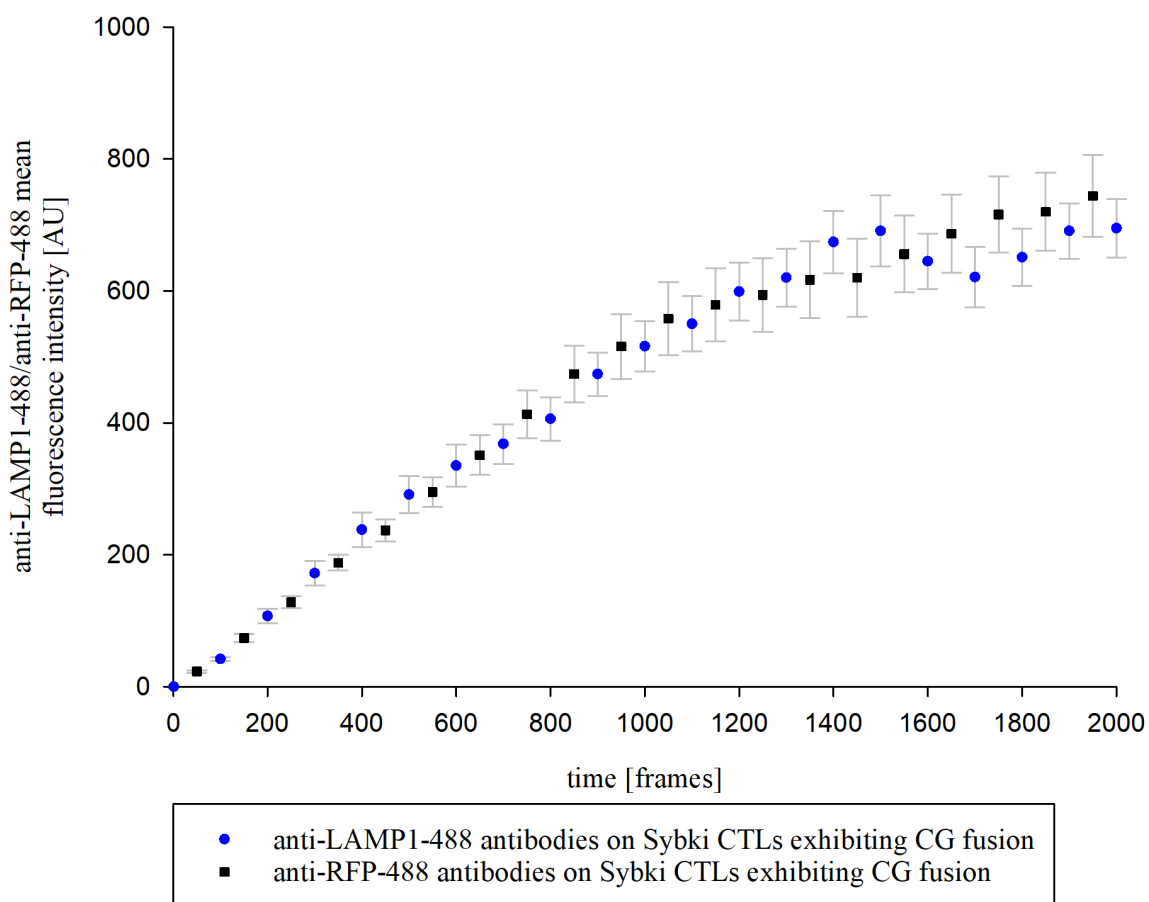


Figure 14. LAMP1 and Syb2 accumulate at a similar rate following CG fusion at the IS.

The similar kinetics of the Syb2 and LAMP1 accumulation at the IS indicate that LAMP1 and Syb2 reach the CTL membrane on a matchable time scale after CG release. Averaged signal of fluorescence of anti-LAMP1-488 (blue dots) and anti-RFP-488 (black squares) over time. Error bars represent SEM. N=3, n=20 (anti-LAMP1), n=27 (anti-RFP).

7.2 ENDOCYTOSIS OF SYNAPTOBREVIN2

7.2.1 Endocytosis of Syb2 takes place within cSMAC and pSMAC

We analyzed the endocytosis of Syb2 by quantifying the disappearance of a clear anti-RFP-488 signal from the TIRF plane over time. For this approach to be valid, we had to rule out lateral diffusion of Syb2 as well as bleaching of the fluorophores.

We ruled out lateral diffusion of fluorescence because we observed no increase in fluorescence around the site of vesicle fusion. Fusion events were counted as endocytosis when lateral diffusion could be ruled out.

We eliminated bleaching as a possible factor of loss of fluorescence by a bleaching test: Bleaching curves revealed only minimal bleaching under our experimental conditions. Furthermore, if the observed endocytosing granule vanished due to bleaching, the signal of surrounding granules should be decreasing as well, which was not the case.

Figure 15 depicts the endocytosis of Syb2 after CG fusion. Cells prepared as described in the previous section were seeded onto the lipid bilayer system and recorded by TIRFM, as described in section 6.5.1. The fluorescence of anti-RFP-488 antibodies was measured.

We observed that endocytosis takes place within the cSMAC (see fig 15 **B**) as well as within the pSMAC (see fig 15 **A**). We defined the pSMAC using fluorescently labeled ICAM1 in the bilayers. Formation of the IS includes association of ICAM1 with LFA1 on the CTL membrane. These two molecules form a ring after IS formation (Dustin, 2015). We determined the inner boundary of the ICAM-405 signal, which is incorporated in our lipid bilayer system as our reference for the cSMAC (see section 4.3 for the bullseye pattern of the SMAC segregation). As the pSMAC is a broader area, endocytic events that happen outside of our reference line likely took place in the pSMAC area.

Results

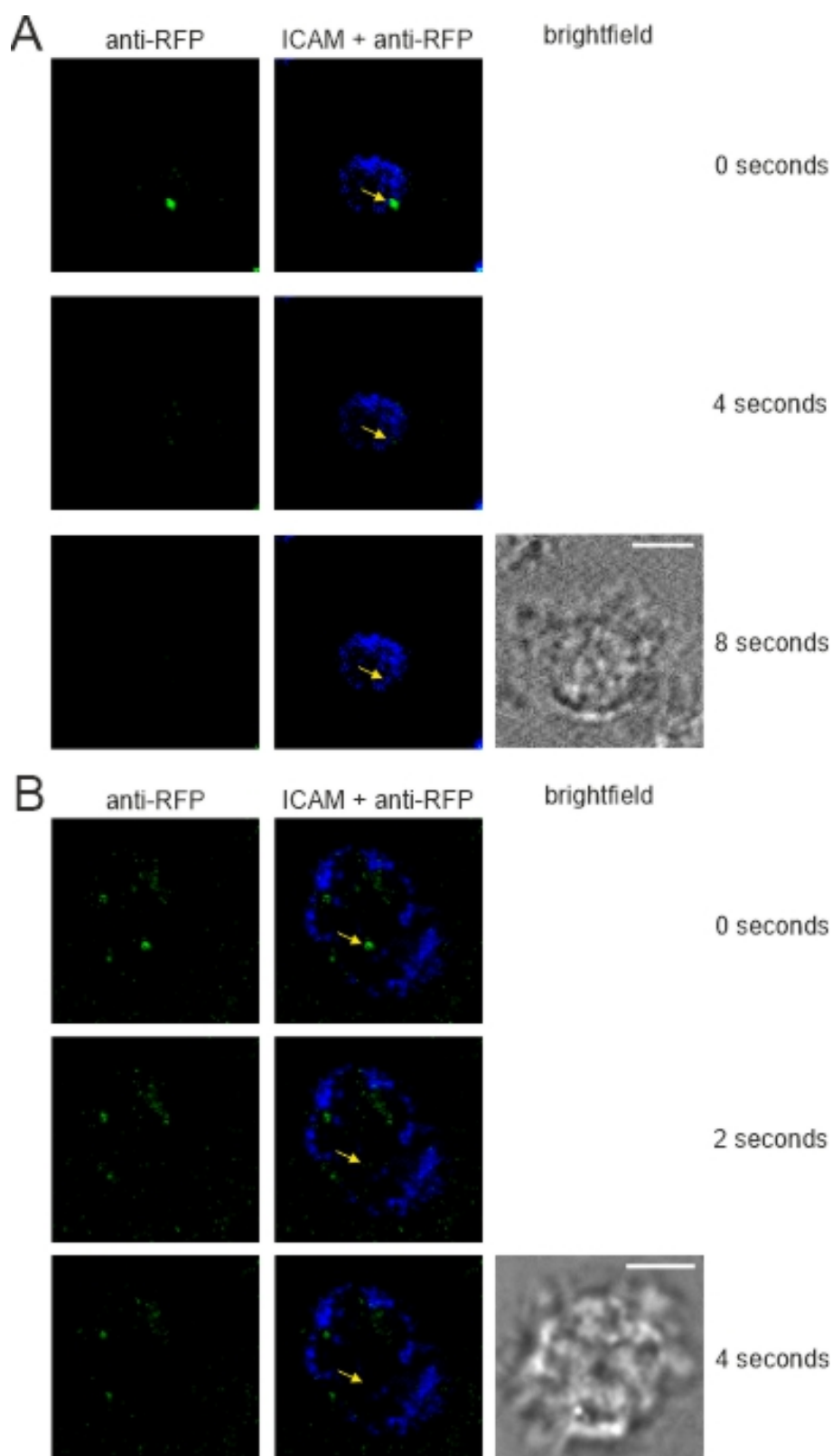


Figure 15. Endocytosis of Syb2 after CG fusion occurs in a central (B) and a peripheral area (A).

The yellow arrows point towards the endocytic event of Syb2 (anti-RFP-488 antibodies, green signal) relative to the ICAM1-405 molecules (blue signal). Sybki cells were plated on the lipid bilayer in a 0 mM calcium extracellular solution and then flushed with a 10 mM calcium buffer containing anti-RFP-488 and imaged in TIRF. The cells were excited by the 488 and 561 lasers with an interval of 100 ms to record anti-RFP-488 and Sybki fluorescence, snapshots to capture the ICAM1 fluorescence were taken at 405 nm after the recording ended. Acquisition frequency: 5 Hz per channel. Scale bar 5 μ m.

Results

The location of the endocytic events relative to the ring-like boundary is depicted in figure 16. The distribution of the endocytic events in pSMAC and cSMAC is nearly equal ($50.98 \pm 7.17\%$ at the cSMAC, $49.01 \pm 7.17\%$ at the pSMAC, total of 86 endocytic events, $n=20$, $N=3$). This result indicates that endocytosis occurs both at the cSMAC and the pSMAC. Mann-Whitney-U test 198, $P = 0.967$.

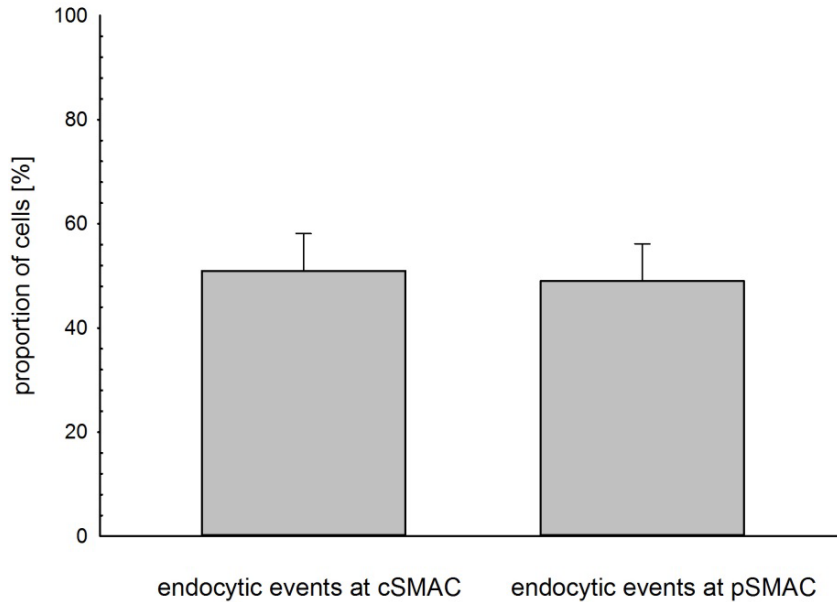


Figure 16. Endocytic events take place at both the cSMAC and the pSMAC.

The proportion of endocytotic events occurring at the cSMAC and pSMAC are similar. Error bars represent SEM, Mann-Whitney-U test 198, $P = 0.967$. $N=3$, $n=86$ (vesicles).

7.2.2 Central endocytic events happen at a hotspot

Figure 17 shows a cluster of anti-RFP fluorescence appearing and staying in the TIRF field after CG fusion. We defined a cluster as an aggregation of anti-RFP fluorescent signals having a $1 \mu\text{m}$ radius, a higher mean fluorescence intensity than the mean intensity of the whole cell, and temporal stability of at least 5 minutes. Of 20 analyzed cells, 16 cells (84.21%, $N=3$) matched these criteria.

We prepared the cells as described in section 6.5.1 and seeded them onto the lipid bilayer system. We recorded the cells by TIRFM, as described in section 6.5.2, using anti-RFP-488 containing extracellular solution.

Results

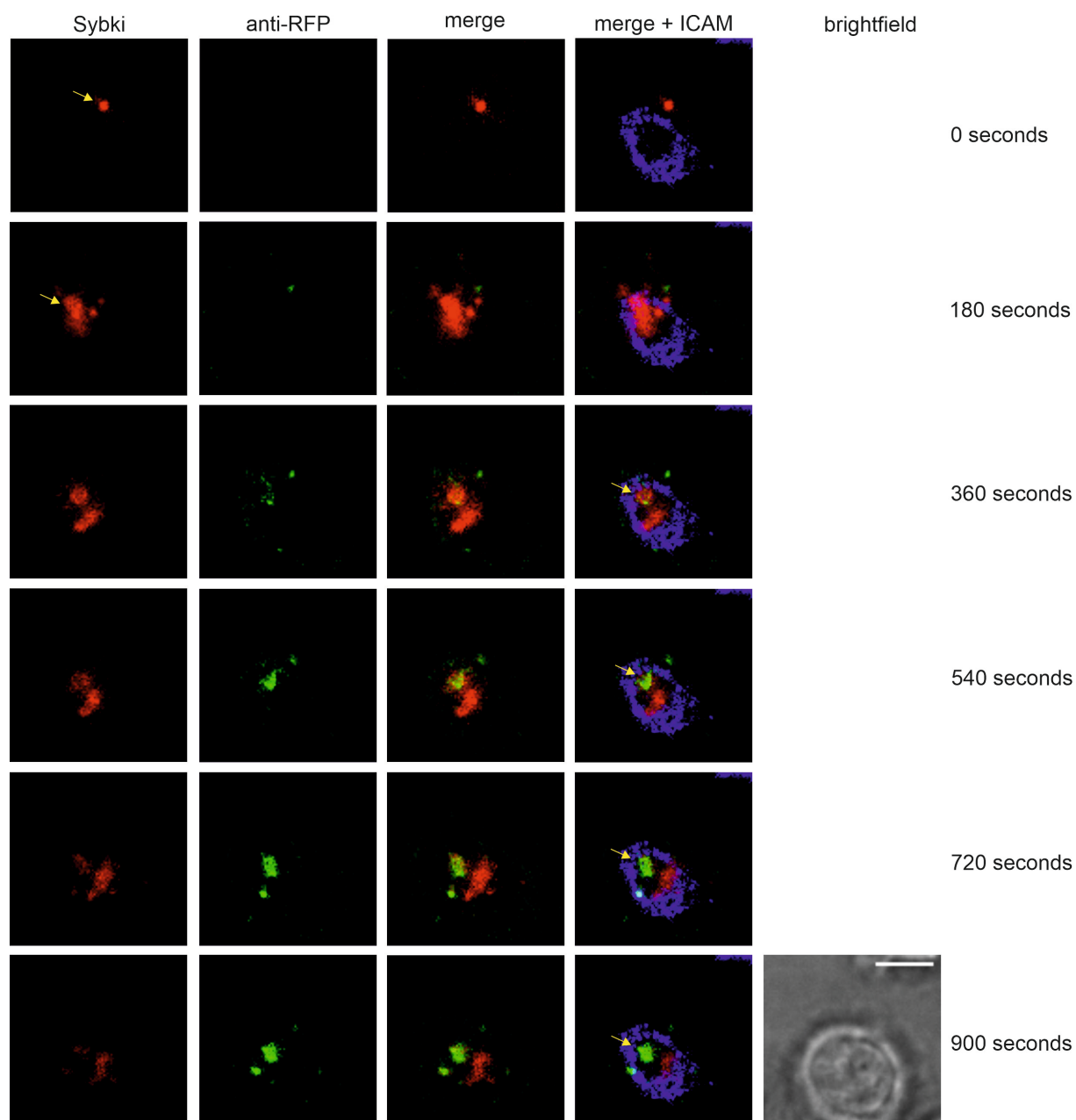


Figure 17. Anti-RFP-488 is observed as a cluster at the cSMAC following CG fusion.

Yellow arrows at 0 and 180 seconds in the Sybki channel point to CGs that will fuse. Yellow arrows at 360, 540, 720 and 900 seconds in the merge + ICAM channel point to the anti-RFP cluster located at the cSMAC. Sybki cells were settled on the lipid bilayer in a 0 mM extracellular calcium solution and then flushed with a 10 mM calcium buffer containing anti-RFP-488 antibodies and imaged in TIRF. The cells were excited by the 488 and 561 lasers with an interval of 100 ms to record anti-RFP-488 and Sybki fluorescence, snapshots to capture the ICAM1 fluorescence were taken at 405 nm after the recording ended. Acquisition frequency: 5 Hz per channel. Scale bar 5 μm .

To analyze whether most endocytic events at the cSMAC take place close to the defined cluster, we measured the distance between the endocytic events and the center of mass (CM) of the cluster. We also measured the radius of the cluster. The mean distance of the endocytic events from the CM of the cluster is $2.25 \pm 0.29 \mu\text{m}$, whereas the radius of the cluster is 2.52 ± 0.21 . From our data, we can conclude that the majority of the Syb2 endocytic events take place within or close to the cluster of anti-RFP-488 (N=3, n=18).

Results

In figure 18, we calculated the area of the cluster and compared it to the area surrounded by the pSMAC (left bar) and the area occupied by the flattened CTL in the TIRF plane (right bar). The area occupied by the whole cell in TIRF was determined by the area which was free from background fluorescence of the anti-RFP-488 antibodies in the extracellular solution. The cluster occupies $40.66 \pm 3.91\%$ of the area surrounded by the pSMAC and $3.86 \pm 0.60\%$ of the area of the whole cell (Mann-Whitney-U test $U = 0$, $P = <0.001$). 68.75% of the central endocytic events take place in this cluster. This indicates that the cluster of anti-RFP accumulation is a well-defined area situated within the boundaries of the pSMAC in which the majority of Syb2 endocytosis events take place.

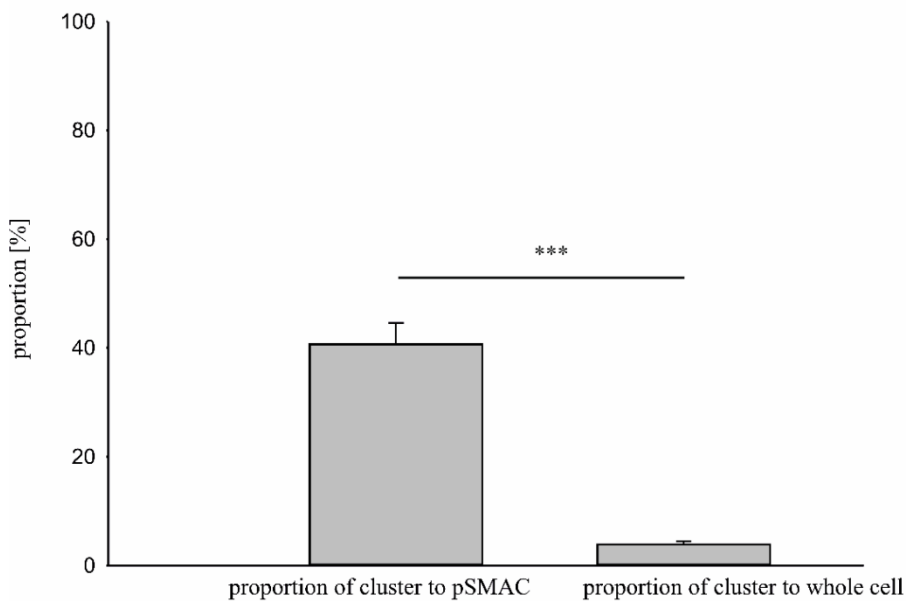


Figure 18. The area of endocytic clusters relative to the area surrounded by the pSMAC (left) and the area of the whole cell (right).

The area of the cluster is equal to $40.66 \pm 3.91\%$ of the area surrounded by pSMAC, whereas the cluster is equal to $3.86 \pm 0.60\%$ of the area of the whole cell visible in the TIRF plane. 68.75% of the endocytic events in the cSMAC happen within this cluster, although the cluster only occupies 3.86% of the area of the whole cell. Error bars represent SEM, Mann-Whitney-U test $U = 0$, $P = <0.001$. $N=3$, $n=18$.

From figures 17 and 18, we can conclude that the observed clusters are hotspots of endocytosis in CTLs and are situated in the cSMAC; we refer to this cluster as a central endocytic zone (CEZ).

Results

7.2.3 Endocytosis of Syb2 at the cSMAC is located close to the area where CG fusion occurs

We next calculated the distance of the center of the proposed CEZ to the average center of all exocytotic fusion events in each CTL. We compared this distance to the average diameter of the pSMAC and of the whole cell (see figure 19).

The average distance between the CEZ and the exocytic area is $1.74 \pm 0.23 \mu\text{m}$. The average radius of the pSMAC is $7.64 \pm 0.34 \mu\text{m}$. Compared to this, the average radius of the whole CTL is $12.83 \pm 0.44 \mu\text{m}$ in our experimental conditions.

We conclude that central endocytic events in CTLs take place in an area located close to the area where CG exocytic events at the cSMAC occur.

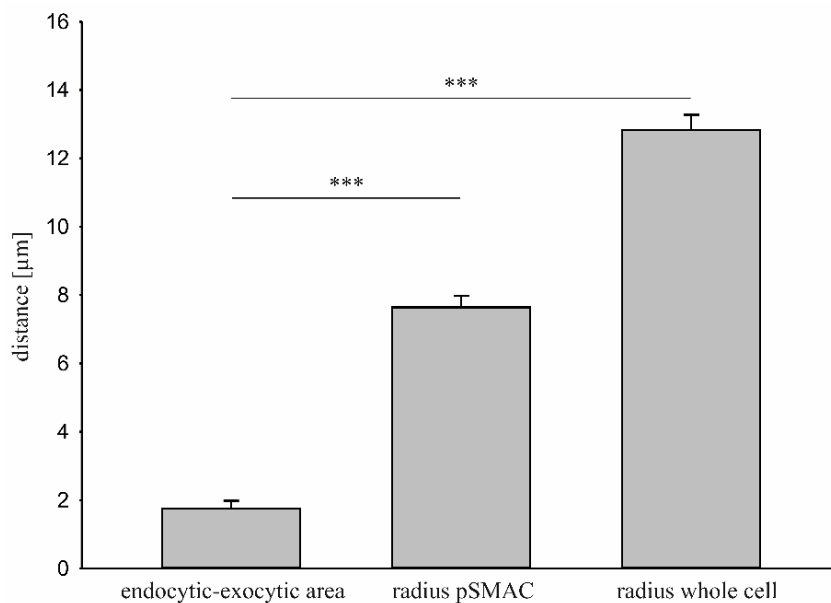


Figure 19. Central endocytic events take place close to area of CG exocytosis.

The distance between endocytic events within the cSMAC to the area of CG exocytosis events (left), to the radius of the pSMAC (middle bar) and to the radius of whole cell (left bar). Error bars represent SEM, Mann-Whitney-U tests $U = 16$, $P = <0.001$ and $U = 0$, $P = <0.001$. $N=3$, $n=21$ (left bar), $n=20$ (middle bar), $n=22$ (right bar).

Results

7.2.4 Syb2 endocytosis occurs in the time range of clathrin-mediated endocytosis

We used the semi-automated mode of the TrackMate tool, an image analysis plug-in for Fiji/ImageJ (see section 6.5.3), to track single anti-RFP-488 puncta in Sybki cells after CG fusion. Cells were prepared and recorded as described in section 6.5.1 and 6.5.2.

Figure 20 depicts the time between the appearance of the Syb2 puncta in TIRF (indicated by the anti-RFP-488 antibodies) and their disappearance. As discussed in section 7.2.1, this disappearance could, in principle, be due to endocytosis, bleaching or lateral diffusion. We ruled out bleaching and lateral diffusion as explained in this section.

Most endocytic events are in the range from 11.6 seconds to 312.4 seconds (71.4%), which is reported as the duration of CME (Watanabe & Boucrot, 2017). We could track 29.6% of the Syb2 puncta for more than 548.6 seconds. Interestingly, no Syb2 puncta appear for less than 11.6 seconds. We conclude that CME is likely involved in the recycling of Syb2 after CG fusion, whereas we did not observe ultra-fast endocytosis.

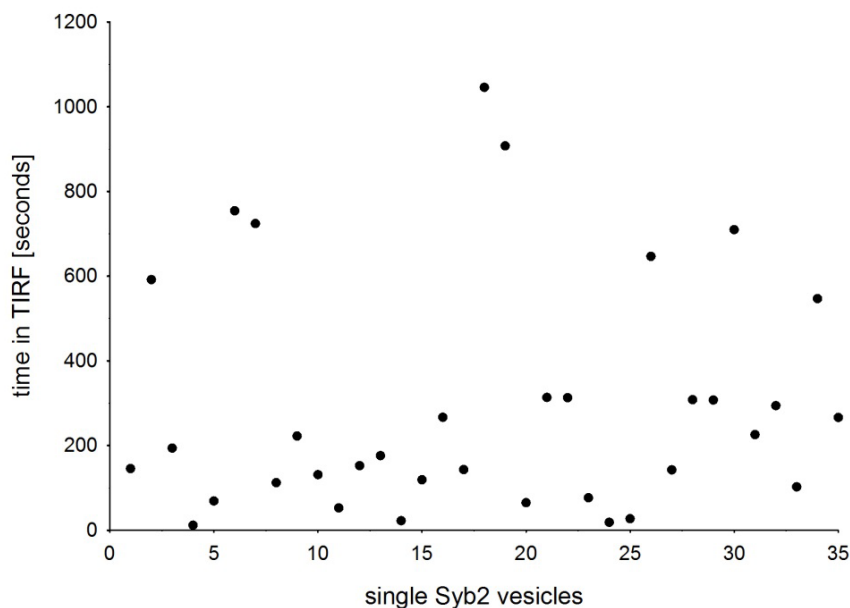


Figure 20. Dwell time of Syb2 puncta after CG fusion indicates CME as possible mechanism involved in their reuptake.

We tracked single Syb2 puncta (black dots) from their appearance after CG fusion to their disappearance at an excitation wavelength of 488 nm. Acquisition frequency: 5 Hz per channel. N=3, n=20.

8 DISCUSSION

In this work, I used TIRF microscopy to visualize CG behavior at the IS formed between CTLs and anti-CD3 and ICAM containing lipid bilayers and subsequently visualized CG endocytosis. I used Syb2 knock-in mice in which the v-SNARE protein Syb2 is endogenously labeled with mRFP. CTLs were stimulated to produce a fusion of CGs so that a subsequent CG endocytosis could be visualized using fluorescently labeled anti-RFP to track Syb2 and anti-LAMP1 to track LAMP1.

I demonstrated that the proteins LAMP1 and Syb2 are markers that can be used to visualize CTL degranulation in mouse CTLs, but that only Syb2 is a specific marker for CG membrane exocytosis. Syb2 is suitable to follow individual endocytic events at the IS in real time. I described the location and timing of subsequent endocytic events of Syb2: There is a central and a peripheral zone of endocytosis within the IS. The central endocytic region is located at the cSMAC in an area close to the well-studied CG exocytic zone. The peripheral region of endocytosis is situated at the pSMAC. Furthermore, I could show that the reuptake of Syb2 is in the time range of CME.

In further experiments, one could try to observe the behavior of clathrin and dynamin, two well-known endocytic proteins, along with endocytosed Syb2. This experiment would be to investigate whether there is a difference in the endocytic mechanism occurring at the central and the peripheral zone.

8.1 CYTOTOXIC GRANULE ENDOCYTOSIS – THE INITIAL SITUATION

Chang et al. have shown that CG endocytosis is required for the efficient killing of multiple target cells by CTLs (Chang et al., 2017). For their studies, they used CTL and target cell conjugates in combination with anti-LAMP1 and anti-RFP antibodies in live-cell confocal fluorescence microscopy. Chang et al. identified anti-RFP antibodies as a specific marker for CG endocytosis in Sybki mice. They also used anti-LAMP1, which was found to be less accurate for CG endocytosis in comparison to anti-RFP antibodies (Chang et al., 2017).

The idea of my experiments is to use a lipid bilayer to mimic a target cell and utilize TIRFM so that we observe each endocytic event at a higher temporal and spatial resolution to gain new insights about the location of CG membrane endocytosis and thus the structure of the IS.

8.2 SYB2 AND LAMP1 EXOCYTOSIS

CTLs, as part of the adaptive immune system, make use of the perforin-killing pathway to eradicate target cells. To do so, they need to release CGs containing perforin and GRZMB (Smyth et al., 2001). This CG release is a well-studied and tightly regulated process in which Syb2 plays a vital role: Matti et al. found that Syb2 is the v-SNARE in mouse CTLs (Matti et al., 2013). Additionally, Matti et al. showed that the size of Syb2-positive vesicles is homogeneously distributed around ~320 nm in diameter and that an electron-dense core structure supposedly constituting the matrix that contains

Discussion

GRZMB and perforin is present (Matti et al., 2013). These features make Syb2 suitable as a functional readout for CG release (and subsequent reuptake) in our studies. LAMP1 is a widely used degranulation marker, which we used as a control (Andrews, 2017).

8.2.1 Syb2 as a marker for CG exocytosis

In neurons, two modes of synaptic vesicle fusion are known: Full-collapse fusion and kiss-and-run fusion (Harata et al., 2006). During a full-collapse fusion, the vesicle membrane is brought tightly together with the outer cell membrane until the vesicle finally spreads out and integrates into the plasma membrane (Harata et al., 2006). During kiss-and-run fusion, a fusion pore forms between the vesicle and the plasma membrane, allowing the cargo of the vesicle to pass through this pore. After the release of the load, a small part of the vesicle membrane remains in the plasma membrane, whereas the major part of the vesicle buds off of the plasma membrane and can fuse again (Harata et al., 2006). In contrast to full-collapse fusion, a certain amount of cargo remains in the vesicle to be released in later fusion events (Harata et al., 2006).

Chang et al. showed that full-collapse fusion is the predominant mode of CG fusion in CTLs in their experimental conditions: They used CTL-target cell conjugates pretreated with the dynamin-inhibitor Dynasore and anti-RFP-488 antibodies. Additionally, GRZMB antibodies were added to the fixed cells after CTL-target cell conjugation (Chang et al., 2017). If there would be kiss-and-run fusion, they expected a co-localization of the GRZMB antibodies and the anti-RFP-488 antibodies within the remaining parts of the CGs as of the remaining cargo in those vesicles. However, Chang et al. did not observe a co-localization indicating full-collapse fusion as the predominant mode of CG exocytosis in CTL-target cell conjugates (Chang et al., 2017). This result is an essential prerequisite to my experiments, as the amount of mRFP molecules released during kiss-and-run fusion is minimal; if this were the primary mode of CG exocytosis, detection of Syb2 using the anti-RFP-488 antibodies in my experiments would be very difficult due to low amounts of antigen. As I use a lipid bilayer built to mimic a target cell by the artificial lipid bilayer coated to the coverslip, I could reasonably assume that the experimental conditions are comparable and that full-collapse fusion is the primary mechanism of CG fusion in my experiments.

I could show that Syb2 accumulates substantially at the IS upon CG fusion and interestingly to a lesser extent upon attachment of the CTL to the lipid bilayer (see figures 9 and 10). The increase of Syb2 after fusion of CGs can be explained by the mechanism of SNARE complexes (see section 4.3): The v-SNARE Syb2 is a vesicular protein that integrates into the plasma membrane upon exocytosis. Since the mRFP moiety of the Syb2-mRFP compound is luminal, after exocytosis the mRFP tag on the cell surface is exposed to the anti-RFP antibodies in the extracellular solution.

The Syb2 accumulation after attachment of the CTL to the lipid bilayer without any CG fusion could be due to increased endocytic sorting of this protein towards the plasma membrane. It has been observed in neurons that the sorting of Syb2 either into synaptic vesicles or the plasma membrane

Discussion

depends on its binding to Synaptophysin1 (Pennuto et al., 2003). If the Syb2 translation increases, the ratio of Syb2 binding to Synaptophysin1 decreases, and more Syb2 is translocated towards the plasma membrane in neurons (Pennuto et al., 2003).

The observation that Syb2 proteins accumulate after attachment but without CG fusion could be due to a similar mechanism in CTLs: Attachment to the lipid bilayer means that the CTL has bound to the anti-CD3 antibodies on the lipid bilayer and recognized the ICAM1 molecules. This recognition leads to activation processes resulting in an increased intracellular calcium concentration and higher protein translation; one of these proteins likely is Syb2, which then integrates into the plasma membrane of the CTL. Since the anti-RFP-488 antibodies bind and accumulate, their antigen, namely RFP molecules, must be on the outer surface, making it likely that it reached the plasma membrane by exocytosis. This indicates a second CG fusion independent pathway of Syb2 release to the CTL's surface; the plasma membrane could act as a storage site for Syb2 proteins. This means that a fraction of newly synthesized Syb2 is exo- and subsequently endocytosed for the use in CG synthesis independent of CG fusion.

It is likely that the fraction of Syb2 proteins, which are integrated into the plasma membrane by CG fusion use the same pathway of endocytosis and are reused to synthesize new CGs. The reuse of synaptic vesicles in neurons is, in principle, comparable: There is a strong relation between endo- and exocytosis of synaptic vesicles, which regulates neuronal synaptic activity (Xie et al., 2017). Xie et al. showed a rise in capacitance at the neuronal membrane (indicating synaptic vesicle exocytosis), followed by a sharp drop in capacitance shortly after, indicating endocytosis using capacitance measurements. Blocking exocytosis with botulinum neurotoxins suppresses endocytosis, which proves the tight coupling of these two processes (Xie et al., 2017).

My finding that a fraction of Syb2 reaches the plasma membrane of CTLs after activation, but irrespective of CG fusion (see figures 9 and 10) has to be compared with earlier results: Matti et al. state that Syb2 is exclusively localized on CGs in mouse CTLs (Matti et al., 2013). They performed structured illumination microscopy (SIM) using Sybki CTLs transfected with GRZMB-TFP and found a co-localization with a Pearson's coefficient of 0.85 (Matti et al., 2013). A Pearson's coefficient of 0.85 means that there is a fraction of Syb2 which does not co-localize with GRZMB; this fraction could be the Syb2 proteins I detected on the membrane irrespective of CG fusion which are stored for endocytosis and synthesis of CGs. My result can, therefore, be seen as a complement to those previous experiments.

Another possible reason why I detected Syb2 in CTL membranes of non-fusing CTLs could be that there were fusion events in cells that I have analyzed as non-fusing, which took place out of the TIRF plane. This possibility seems to be unlikely, though, because there was no substantial increase in fluorescence in non-fusing CTLs using anti-LAMP1 antibodies, which are a well-established

degranulation marker (see figure 12 and section 8.2.2). This indicates the correct discrimination between fusing and non-fusing CTLs in my experiments.

8.2.2 LAMP1 as a marker for CG exocytosis

I could show that an accumulation of anti-LAMP1 antibodies is specific for CTLs exhibiting degranulation, but that the anti-LAMP1 antibodies do not specifically detect CG membrane fusion (see figures 12, 13 and 14). This is in line with the use of anti-LAMP1 antibodies as degranulation markers in FACS analyses (Andrews, 2017). As there is only a weak co-localization between the endogenous Sybki signal and the anti-LAMP1-488 signal (see figure 11), I can conclude that there is an alternative pathway of LAMP1 exocytosis other than the exocytosis via CGs. This finding makes LAMP1 not suitable as a specific marker for CG membrane exo- and endocytosis.

Chang et al. also showed in their studies that Syb2 is a more specific marker for CG exocytosis than LAMP1: They used confocal fluorescence microscopy and CTL-target cell conjugates in combination with anti-LAMP1-488 antibodies and found that LAMP1 is endocytosed at the entire plasma membrane and not only at the IS (Chang et al., 2017). The authors correlated the anti-LAMP1-488 signal with the endogenous Syb2 signal of the Sybki CTL and found a correlation of those two proteins in only one-fifth of the LAMP1-containing vesicle population (Chang et al., 2017). This is also in line with my observations: I could not detect a significant co-localization between the anti-LAMP1-488 antibodies and the endogenous Syb2-488 signal, indicated by a Pearson coefficient of 0.30 (see figure 11). These results point out that there is either a different amount of those proteins expressed in CGs or that there are more LAMP1-positive and Syb2-negative vesicles than LAMP1-positive and Syb2-positive ones. To find the reason, Chang et al. determined the total number of LAMP1-positive and Syb2-positive vesicles during their recordings and found twice as many LAMP1-positive vesicles indicating that conventional lysosome secretion could explain the finding rather than disparate protein concentrations in CGs (Chang et al., 2017).

In contrast to the anti-RFP antibodies, there is almost no accumulation of anti-LAMP1 visible in non-fusing CTLs (see figures 9, 10, 12, 13). This indicates that there is no sorting of LAMP1 to the cell membrane when the CTL does not degranulate, consistent with its use in degranulation essays.

8.2.3 Kinetic aspects of LAMP1 and Syb2 accumulation after CG fusion

LAMP1 and Syb2 show comparable rates of aggregation at the IS after CG exocytosis (see figure 14). As they are both constituents of CGs (Peters et al., 1991) (Matti et al., 2013) they should both integrate into the plasma membrane of the CTL at the same time during CG fusion. The aggregation of the two antibodies on a similar time scale leads to the conclusion that they both reside on the CG membrane. This result is in line with the literature and demonstrates that the majority of Syb2 and LAMP1 in the plasma membrane is derived from CGs. It is another independent prove that Syb2 is a suitable marker of CG fusion, as it is exocytosed with the well-established degranulation marker LAMP1.

Discussion

As mentioned above, there is an increase in fluorescence of anti-RFP-488 antibodies in CTLs independent of CG fusion (see section 8.2.1). Regarding the kinetics of Syb2 and LAMP1 accumulation, it is likely that the CG fusion independent Syb2 at the CTLs surface is a smaller fraction of the total amount of Syb2 in the membrane. This small amount of antigen could explain why it was not detected beforehand by Matti et al.

The time-span (~13 minutes) between the first event of CG fusion and the maximum anti-LAMP1 and anti-RFP signal is likely because more than one CG fusion, or in case of the alternative LAMP1 exocytosis pathway more than one vesicle fusion event occurs during the recording (average of 2.6 ± 0.7 CG fusion events per cell, data not shown). This means that more CGs or vesicles containing LAMP1 and Syb2-mRFP integrate into the membrane during the recording, which is expected.

8.3 ENDOCYTOSIS OF SYNAPTOBREVIN2

CTLs defend the human body against viral infections and tumor cells. To do so, they need to be capable of highly efficient killing of target cells. They obtain this capability by distinct mechanisms of CG delivery: parallel and serial killing as well as fast CG delivery (Isaaz et al., 1995) (Wiedeman et al., 2006). Though these exocytic mechanisms have been studied in great detail, the subsequent reuptake of membrane components has only recently found to be highly relevant for the multiple killing of target cells by CTLs: Chang et al. have shown that CTL membrane components are reused and, for that reason, refilled with cytotoxic substances such as perforin and GRZMB (Chang et al., 2017). Building on this, it was the aim of my experiments to study this process in greater detail at the IS.

The results indicate that the endocytosis of Syb2 occurs in two distinct areas in the IS: in a central area located at the cSMAC and a peripheral zone at the pSMAC (see figure 15); roughly the same proportion of endocytic events takes place in the central and peripheral area (see figure 16). The central endocytic area is located close to the well-described area of CG exocytosis (see figure 19) (Griffith, 2012). This is comparable to the membrane retrieval in neurons: CME occurs at peripheral regions of the neuronal synapse away from the active zone, whereas bulk endocytosis has been shown to take place close to the active zone (Li & Venkatesh, 2001).

There is support for the idea of a central endocytic zone in CTLs in the literature: Das et al. performed confocal fluorescence microscopy with Jurkat CTL-APC conjugates (Das et al., 2004). They used fluorescently labeled transferrin receptors as a marker for endocytosis (known for perpetual recycling from the cell surface) and fluorescently labeled TCRs. Das et al. found a strong co-localization between the transferrin receptors and the TCRs in case of stimulation with superantigen-pulsed APCs (Das et al., 2004). This indicates that there is an endocytic zone in the area of the TCR, which is located within the cSMAC, supporting my data of a central endocytic zone.

Discussion

Additionally, most central endocytic events (within the cSMAC) happen in an area of high Syb2 concentration (see figures 17 and 18). This could indicate the retrieval via bulk endocytosis. In the peripheral endocytic zone, there is no such cluster of Syb2 visible. This difference could suggest that two different mechanisms of endocytosis retrieve Syb2 at the IS, making it similar to the reuptake of neurotransmitters in neuronal cells. It has been shown that both, clathrin-mediated endocytosis and bulk endocytosis, take place in neuronal cells (Gross & Gersdorff, 2016): Gersdorff et al. used pH-sensitive dyes in combination with fluorescence imaging to track the time course of pH changes upon neuronal cell stimulation; they found a span of endocytic events matching CME as well as bulk endocytosis depending on the strength of the stimulus (Von Gersdorff & Mathews, 1994).

In my experimental conditions, the dwell time of the majority of the Syb2 puncta in TIRF (11.6 seconds to 312.4 seconds) supports CME as the main mechanism of Syb2 endocytosis (see figure 20) (Watanabe & Boucrot, 2017). Chang et al. found a similar time range of Syb2 retrieval in their experiments using CTL-target cell conjugates and confocal fluorescence microscopy (Chang et al., 2017). This makes CME likely to be one of the endocytic pathways of CG membrane retrieval, although more experiments must be performed to prove this strong indication (see section 8.4).

It is known for neurons, that CME is the predominant mode of endocytosis in resting cells, but clathrin-independent fast pathways such as kiss-and-run and ultrafast endocytosis are triggered after the release of neurotransmitters (Watanabe & Boucrot, 2017). That makes sense, as the average amount of cargo endocytosed via CME is limited (the exact number depends on the substrate). Borner et al. used proteomic methods and HeLa-cells to calculate the amount of small mannose 6-phosphate receptors (M6PR) endocytosed by one clathrin-coated pit and found that to be roughly 30 M6PRs per pit (Borner et al., 2012). Thus, it would take dozens of minutes to remove specific receptors (some of them more than one million copies at a time on the cell surface) from the cell membrane (Watanabe & Boucrot, 2017). Applied to this study, it illustrates that there are likely faster methods to clear CG membrane components such as Syb2 from the cell surface than CME. This is because the CTLs rely on the reuse of those membrane components for efficient killing of target cells in the time frame of a few minutes (Chang et al., 2017).

The lipid bilayers used in this study were coated with anti-CD3 antibodies at a concentration of 20 $\mu\text{g/ml}$. Torres et al. used a concentration of 1 $\mu\text{g/ml}$ of anti-CD3 antibodies to study the formation of the IS and organization of TCRs, indicating that the concentration I have used for the studies on CG endocytosis is a potent stimulus for the CTLs (Torres et al., 2012). A stronger stimulation leads to a higher amount of CGs released by the CTL (data not shown), which implies that much more CG membrane compartments need to be recycled. Hence it makes sense that fast endocytosis is occurring under the experimental conditions in this study in addition to CME to effectively clear Syb2 from the CTL's surface. We were not able to detect this fast mode of endocytosis due to the limitations of our

Discussion

experimental setting (see section 8.4), nevertheless it seems to be a possibility that those processes occur in CTLs. For suggestions on how to improve the experimental parameters, see section 8.4.

Houy et al. reported on a mechanism which enables neuroendocrine cells to sustain homeostasis of their cell and vesicular membranes through vesicular trafficking (Houy et al., 2013). The model of full-collapse fusion involves the complete integration of the vesicular membrane into the plasma membrane (see 8.2.1) (Harata et al., 2006); so far, the scientific consensus was that the subsequent endocytosis by either CME or bulk endocytosis randomly picks up parts of the plasma membrane (Houy et al., 2013). The endocytosed lipids and proteins would then be sorted and reassembled to be reused in the synthesis of vesicles. This model conflicts with findings that neither the vesicular proteins disperse over the entire plasma membrane nor that more considerable amounts of plasma membrane were found in synaptic vesicle membranes (Rizzolo & Jahn, 2007). The new model introduced by Houy et al. assumes a function of lipids like cholesterol and phosphatidylinositol 4,5 bisphosphate [PI(4,5)P₂] in the formation of lipid rafts which prevent proteins and lipids derived from synaptic vesicles to distribute among the entire plasma membrane (Houy et al., 2013). Those microdomains can subsequently be endocytosed without mingling with other cell membrane constituents. Houy et al. labeled the granule membrane protein dopamine- β -hydroxylase (DBH) with an antibody against the luminal region to follow the endocytosis of vesicles that underwent full-collapse fusion in chromaffin cells. They observed that the protein DBH clusters in an area close to the site of exocytosis among other specific granule indicators and is then endocytosed through vesicles formed predominantly of granule constituents using electron microscopy and TIRFM. This nascent vesicle then merges with an early endosomal compartment in an actin- and clathrin-dependent manner. The process of microdomain formation on the plasma membrane and specific reuptake of the preserved granule domain simplifies a selective sorting of granule membrane constituents (Balseiro-Gomez et al., 2016).

A comparable model has been introduced by Bittner et al.: They postulated a nibbling mechanism of the clathrin-mediated endocytosis of secretory granules after fusion with the plasma membrane (Bittner et al., 2013). The authors found a size discrepancy between chromaffin granules and clathrin-coated vesicles (~300 nm vs. ~90nm). Their data further shows that the granule membrane is preserved as a moiety in the plasma membrane after exocytosis and provides a spot of nucleation for clathrin- and dynamin-dependent reuptake (Bittner et al., 2013). This indicates that fused granules cannot be endocytosed en bloc; and they proposed that the reuptake is instead based on a piece by piece mechanism mediated by clathrin and dynamin.

I observed a similar phenomenon in my experiments: After CG fusion, a significant confluence of Syb2 signal enriches at the site of CG fusion (see figures 17 and 18). This observation indicates that the CG membrane components do not distribute among the plasma membrane, but stay in the area of CG fusion. This observation is in line with the discovery of Houy et al. of microdomain formation

Discussion

after synaptic vesicle exocytosis in chromaffin cells (Houy et al., 2013); it would make sense that there is an analogous mechanism in CTLs.

Data from Chang et al. supports this finding: They used palmitoylated Gcamp6f (palmpalm-Gcamp6f) as a calcium sensor in combination with TIRFM and anti-CD3 coated glass coverslips to quantify the calcium level at the IS in CTLs. Palmpalm-Gcamp6f consists of the calcium sensor Calmodulin and a green fluorescence protein (GFP), in which fluorescence intensifies after calcium cations form complex bonds with Calmodulin. They found an increased calcium signal upon binding of the CTL to the anti-CD3 coated glass coverslip as well as a change in the shape of the cell, indicating the recognition of the antigen (Chang et al., 2017). After the detection of the antigen, CGs polarize towards the IS and fuse vesicles containing GRZMB at the plasma membrane (Chang et al., 2017). The authors showed the complete disappearance of several GRZMB containing vesicles at the IS demonstrating the full-collapse exocytosis and fusion with the plasma membrane. Seconds after the fusion process, they observed an expansion of the granule membrane due to the full-collapse exocytosis. This was followed by a sharp increase of the palmpalm-Gcamp6f fluorescence intensity around this spot indicating a high calcium concentration (Chang et al., 2017). During the next seconds, they could detect the closing of the fusion pore accompanied by a steady rise of the calcium signal around the fusion pore (Chang et al., 2017). After ~5 mins in which the endocytosis of the CG supposedly takes place, they state that the palmpalm-Gcamp6f signal completely vanished. In their study, Chang et al. used anti-CD3 coated glass coverslips, which present the CTL a relatively inflexible target membrane limiting the significance of this result. In combination with my findings using the artificial lipid bilayer as a target cell membrane, which overcomes this drawback by providing a highly flexible layer to the CTL, the significance of these results is increased: Combining those results, it seems likely that the CG membrane components stay in microdomains at the plasma membrane after CG fusion and that subsequent endocytosis takes place close to the area of CG exocytosis in CTLs. This would be comparable with the behavior of vesicles exocytosed in neuroendocrine cells referred to earlier (Houy et al., 2013).

8.4 LIMITATIONS AND OUTLOOK

In this study, I have elucidated new insights into the process of CG membrane retrieval at the IS: I could deepen the understanding of this mechanism, especially regarding temporal and spatial resolution. I found that the CG membrane constituent Syb2 is retrieved at two different areas at the IS, a central and a peripheral region. Additionally, I could demonstrate that the CG endocytosis occurs within the time range of CME meaning in the dimension of dozens of seconds.

The experiments discussed in this thesis were acquired with CTLs incubated and prepared for the recording as described in section 6.5.1 and 6.5.2: The anti-RFP-488 and anti-LAMP1-488 antibodies were added to the cell suspension on the lipid bilayer by the time of the recording. As the CTLs settled

Discussion

and attached to the lipid bilayer, they displaced the fluorescent extracellular solution on the lipid bilayer in the TIRF plane. Outside of the cell outline, the fluorescent antibodies induced a high background noise, whereas the IS was almost free of background due to the displacement of the extracellular solution. As the IS is the area I am interested in, this method is sufficient to perform the experiments discussed in this thesis. Besides the drawback concerning the signal to noise ratio, this method has another substantial disadvantage: The anti-LAMP1 and anti-RFP antibodies must diffuse from the extracellular fluid to the IS where the binding to the CG membrane can take place after CG fusion. I assume that this process is mainly responsible for the delay in the detection of the Syb2 and LAMP1 signal after CG fusion (see figures 8 and 11). Logically, a setting in which there is less background noise and no delayed binding of the antibodies is preferable: I incubated the CTLs with the anti-RFP-488 antibodies for several minutes and replaced the extracellular fluid containing the antibodies before the recording. The idea of this procedure was that the anti-RFP-488 antibodies bind to the small amount of Syb2, which is constitutively part of the CTL membrane and would then enrich in the areas of higher Syb2 concentration as soon as a CG fusion took place. This would offer the advantage of lower background noise, as the extracellular fluid is free from antibodies as well as instantaneous binding of the antibodies as they evenly distribute among the CTL surface. Unfortunately, the procedure turned out not to work as I have observed the Syb2 signal endocytosed in the CTL before the attachment of the CTL to the lipid bilayer. I suspect that the high amount of extracellular anti-RFP-488 antibodies in the extracellular fluid led to constitutive endocytosis of the antibodies by the CTL regardless of CG fusion. These constitutively endocytosed anti-RFP-488 antibodies cannot be distinguished from those antibodies, which bind to the Syb2 released and endocytosed upon CG fusion, making this approach not suitable for my studies.

I first performed an extensive series of experiments using CTLs cultured for 3 consecutive days after isolation. For this, I applied the same protocol regarding the preparation of the cells for TIRF measurements as described in section 6.5.1 and performed the same experiments with anti-RFP-488 and anti-LAMP1-488 antibodies, as described in 6.5.2. I observed similar results in respect of the specificity of the anti-LAMP1-488 signal in fusing versus non-fusing CTLs and could visualize endocytosis of anti-LAMP1-488 following CG fusion (data not shown). However, this was not valid for the use of the anti-RFP-488 antibody: I could not see any significant difference in fluorescence intensity between fusing and non-fusing CTLs and subsequently no specific Syb2 endocytosis in TIRF due to a very low signal intensity (data not shown).

Because of my observations regarding the lack of specificity of the LAMP1 antibodies for CG membrane exocytosis (see 8.2.2), I could not use LAMP1 as the marker for CG membrane endocytosis. Instead, I intended to use anti-RFP antibodies to more accurately track CG endocytosis. There were three options to overcome the problem above of the low anti-RFP-488 signal intensity: Either to increase the amount of anti-RFP-488 antibodies, to improve the signal intensity of each anti-RFP-488 antibody or to provide the antibodies with more antigens. By increasing the concentration of

Discussion

the anti-RFP-488 antibodies, the signal to noise ratio worsened noticeably: As I applied the antibodies extracellularly, the higher fluorescence intensity of the extracellular solution prevents meaningful analysis of the anti-RFP-488 signal within the IS. To increase the signal intensity of each anti-RFP antibody, I used FluoTag-X4 anti-mRFP antibodies, which are a combination of two antibodies recognizing two distinct epitopes of the mRFP molecule. Each of those two site-specific antibodies is coupled to two fluorophores resulting in a total of 4 fluorophores binding to each mRFP molecule. Unfortunately, the analysis of those TIRF recordings showed weak affinity of the mRFP antibodies to the antigen making it impossible to proceed with this approach. To increase the number of antigens the anti-RFP-488 antibodies can bind to, the CTL has to fuse significantly more CGs per cell. Unpublished fluorescence-activated cell sorting (FACS) data using CD44-APC and CD62L-FITC antibodies from our lab indicate that the CTL population shifts from central memory to effector memory cells during anti-CD3/CD28 bead stimulation. Between day 1 and day 5 of the culture, the data indicates a mixed population of the CTLs, whereas, after day 5, the culture almost exclusively consists of effector memory CTLs. Wolint et al. showed that immediate degranulation is significantly higher in effector memory cells compared to central memory cells (Wolint et al., 2004). With my experimental settings, I am mainly observing immediate degranulation, as the recording time is limited to a maximum of 20 minutes; often, CTLs settle throughout the recording so that the span in which the CTLs are observed is even less. In order to provide the anti-RFP-488 antibodies with more antigen, I conducted TIRF recordings with CTLs cultured for 8-10 days; this improved the signal intensity so that the Syb2 endocytosis can be followed and analyzed; one has to be aware of the differing CTL population though, when comparing the results with earlier experiments from our lab, especially from Chang et al. who used CTLs cultured for 3 days.

The spatial resolution of the Syb2 endocytosis events (see figures 15 and 16) is undoubtedly improvable: I merged images of the recording of the anti-RFP-488 channel (indicating syb2 proteins) with a snapshot of the ICAM1 channel taken shortly after the record ended. Due to the flexibility which the artificial lipid bilayer provides the CTL with, there is some movement of the cell during the recording possible. I excluded those cells from the analysis, which have moved from their origin by eye. Nevertheless, there is a little shift in the position of the analyzed cells possible. This analysis should be accurate enough to make the statement if the endocytic events happen within or outside of the pSMAC, as well as giving an idea where, within the cSMAC, the endocytosis occurs. A more precise way to collect the positions of the endocytic events would be a triple channel recording in TIRF: 561 nm to catch the CG fusion (Sybki channel), 488 nm to follow the CG endocytosis (anti-RFP-488 channel) and using an ICAM1 molecule labeled with Alexa-647 (instead of Alexa-405). Unfortunately, the TIRF setup used for the present work is not equipped with a laser recording at 647 nm. Due to cross-excitation artifacts, it is not possible to simultaneously record at 488 nm and 405 nm. This is the reason why I took snapshots of the ICAM1 molecules and did not record a full video at 405

Discussion

nm. This issue can be overcome by purchasing an additional laser operating at a wavelength of 647 nm.

It is known from neurons that the mechanism of the neurotransmitter reuptake changes according to the strength of the stimulus, the temperature, and the maturation of the cell (Smith et al., 2008). It would be interesting to see if these conditions affect the reuptake of Syb2 in CTLs. To study different mechanisms of endocytosis and to trace ultra-fast endocytosis, the experimental setting has to be modified. Ultra-fast endocytosis takes milliseconds to a few seconds (Brockmann & Rosenmund, 2016); I could not observe such rapid endocytosis with our experimental settings: The accumulation of the anti-RFP-488 signal takes a few seconds to exceed the detection limit and is too slow to detect ultra-fast endocytosis (see figure 8). In future experiments, a pH-dependent dye could be used to overcome this drawback and to visualize possible ultra-fast endocytic events.

To have a second independent proof of CME as a mechanism of CG endocytosis, visualization of clathrin as a marker of CME in parallel with the endocytosing Syb2 would be necessary. This can be done by transfection of the Sybki CTLs with a gene construct expressing clathrin coupled to a fluorescent dye and subsequent application of the anti-RFP-488 antibodies extracellularly using the same experimental settings as in this study.

Furthermore, the application of clathrin and/or dynamin inhibitors would be interesting to analyze the delay or size of the clusters formed after CG exocytosis. This, in combination with a pH-dependent dye, could help to identify and quantify further mechanisms of CG endocytosis.

9 REFERENCES

1. Andersen M, Schrama D, Straten P, Becker J (2006). Perspective cytotoxic T-cells. *Journal of Investigative Dermatology* 126:32-41.
2. Andrews N (2017). Detection of Lysosomal Exocytosis by Surface Exposure of Lamp1 Luminal Epitopes. *Methods Mol Biol.* 1594:205-211.
3. Balseiro-Gomez S, Flores J, Acosta J, Ramirez-Ponce M, Ales E (2016). Transient fusion ensures granule replenishment to enable repeated release after IgE-mediated mast cell degranulation. *Journal of Cell Science* 129:3989-4000.
4. Beguinot L, Lyall R, Willingham M, Pastan I (1984). Down-regulation of the epidermal growth factor receptor in KB cells is due to receptor internalization and subsequent degradation in lysosomes. *Proc Natl Acad Sci U S A* 81:2384-2388.
5. Bittner M, Aikman R, Holz R (2013). A nibbling mechanism for clathrin-mediated retrieval of secretory granule membrane after exocytosis. *J Biol Chem.* 13:9177-88.
6. Bogle G, Dunbar P (2010). T cell responses in lymph nodes. *Wiley Interdiscip Rev Syst Biol Med.* 2:107-116.
7. Boomer J, Green J (2010). An Enigmatic Tail of CD28 Signaling. *Cold Spring Harb Perspect Biol.* 2:10.1101/cshperspect.a002436.
8. Borner G, Antrobus R, Hirst J, Bhumbra G, Kozik P, Jackson LP, Sahlender DA, Robinson M (2012). Multivariate proteomic profiling identifies novel accessory proteins of coated vesicles. *JCB* 197:10.1083/jcb.201111049.
9. Boswell K, James D, Essquibel J, Bruinsma S, Shirakawa R, Horiuchi H, Martin TFJ (2012). Munc13-4 reconstitutes calcium-dependent. *The Journal of Cell Biology* 197:301-312.
10. Brockmann M, Rosenmund C (2016). Catching Up with Ultrafast Endocytosis. *Neuron* 90:423-424.
11. Chang H, Bzeih H, Chitirala P, Ravichandran K, Sleiman M, Krause E, Hahn U, Pattu V, Rettig J (2017). Preparing the lethal hit: interplay between exo- and endocytic pathways in cytotoxic T lymphocytes. *Cell Mol Life Sci.* 74:399-408.
12. Cornish G, Sinclair L, Cantrell D (2006). Differential regulation of T-cell growth by IL-2 and IL-15. *Blood* 108:600-608.

13. Das V, Nal B, Dujeancourt A, Thoulouze M, Galli T, Roux P, Dautry-Varsat A, Alcover A (2004). Activation-Induced Polarized Recycling Targets T Cell Antigen Receptors to the Immunological Synapse: Involvement of SNARE Complexes. *Immunity* 20:577-588.
14. De Saint Basile G, Sepulveda F, Maschalidi S, Fischer A (2015). Cytotoxic granule secretion by lymphocytes and its link to immune homeostasis. *F1000Res.* 4: 10.12688/f1000research.6754.1.
15. Dustin M (2015). The immunological synapse. *Cancer Immunol Res.* 11:1023-1033.
16. Dustin M, Colman D (2002). Neural and immunological synaptic relations. *Science* 298:785-789.
17. Feldmann J, Callebaut I, Raposo G, Certain S, Bacq D, Dumont C, Lambert N, Ouachée-Chardin M, Chedeville G, Tamary H, Minard-Collin V, Vilmer E, Blanche S, Le Deist F, Fischer A, de Saint Basile G (2003). Munc13-4 is essential for cytolytic granules fusion and is mutated in a form of familial hemophagocytic lymphohistiocytosis (FHL3). *Cell* 115:461-473.
18. Ferguson S, Raimondi A, Paradise S, Mesaki K, Ferguson A, Destaing O, Ko G, Takasaki J, Cremona O, O'Toole E, De Camilli P (2009). Coordinated actions of actin and BAR proteins upstream of dynamin at endocytic clathrin-coated pits. *Dev Cell.* 17:81-822.
19. Flajnik M, Kasahara M (2010). Origin and evolution of the adaptive immune system: genetic events and selective pressures. *Nat Rev Genet.* 11:47-59.
20. Gasteiger G, Ataide M, Kastenmüller W (2016). Lymph node – an organ for T-cell activation and pathogen defense. *Immunological Reviews* 2:107-116.
21. Griffith G (2012). The immunological synapse: a focal point for endocytosis and exocytosis. *The Journal Of Cell Biology* 25:183-189.
22. Gross O, Gersdorff H (2016). Endocytosis: Recycling at synapses. *eLife* 5:10.7554/eLife.17692.
23. Harata N, Aravanis A, Tsien R (2006). Kiss-and-run and full-collapse fusion as modes of exo-endocytosis in neurosecretion. *Journal of Neurochemistry* 97:1546-1570.
24. Henne W, Boucrot E, Meinecke M, Evergren E, Vallis Y, Mittal R, McMahon HT (2010). FCHo Proteins are Nucleators of Clathrin-Mediated Endocytosis. *Science* 328:1281-1284.
25. Houy S, Croise P, Gubar O, Chasserot-Golaz S, Tryoen-Toth P, Bailly Y, Ory S, Bader MF, Gasman S (2013). Exocytosis and Endocytosis in Neuroendocrine Cells: Inseparable Membranes! *Front Endocrinol (Lausanne)* 4:10.3389/fendo.2013.00135.

26. Huang G, Huso D, Bouyain S, Tu J, McCorkell K, May MJ, Zhu Y, Lutz M, Collins S, Dehoff M, Kang S, Whartenby K, Powell J, Leahy D, Worley PF (2008). NFAT binding and regulation of T cell activation by the cytoplasmic scaffolding Homer proteins. *Science* 319:476-481.
27. Isaaz S, Baetz K, Olsen K, Podack E, Griffiths G (1995). Serial killing by cytotoxic T lymphocytes: T cell receptor triggers degranulation, re-filling of the lytic granules and secretion of lytic proteins via a non-granule pathway. *Eur J Immunol.* 4:1017-9.
28. Iwasaki A, Medzhitov R (2015). Control of adaptive immunity by the innate immune system. *Nature Immunology* 16:34-353.
29. Johnson K, Bromley S, Dustin M, Thomas M (2000). A supramolecular basis for CD45 tyrosine phosphatase regulation in sustained T cell activation. *Proc Natl Acad Sci U S A* 97:10138-10143.
30. Kaizuka Y, Douglass A, Varma R, Dustin M, Vale R (2007). Mechanisms for segregating T cell receptor and adhesion molecules during immunological synapse formation in Jurkat T cells. *Proc Natl Acad Sci U S A* 104:20296-301.
31. Klein L, Kyewski B, Allen P, Hogquist K (2014). Positive and negative selection of the T cell repertoire: what thymocytes see (and don't see). *Nature Reviews Immunology* 14:377-391.
32. Kyewski B, Klein L (2006). A central role for central tolerance. *Annu Rev Immunol.* 24:571-606.
33. Le Roy C, Wrana J (2005). Clathrin- and non-clathrin-mediated endocytic regulation of cell signalling. *Nature Reviews Molecular Cell Biology* 6:112-126.
34. Lenardo Y (1991). Interleukin-2 programs mouse $\alpha\beta$ T lymphocytes for apoptosis. *Nature* 353:858-861.
35. Li Z, Venkatesh N (2001). Visualizing Postendocytic Traffic of Synaptic Vesicles at Hippocampal Synapses. *Neuron* 31:593-605.
36. Ma L, Rebane A, Yang G, Xi Z, Kang Y, Gao Y, Zhang Y (2015). Munc18-1-regulated stage-wise SNARE assembly underlying synaptic exocytosis. *eLife* 4:10.7554/eLife.09580.
37. Mardones GA, Burgos PV, Lin Y, Kloer DP, Magadan JG, Hurley JH, Bonafacino JS (2013). Structural Basis for the Recognition of Tyrosine-based Sorting Signals by the μ 3A Subunit of the AP-3 Adaptor Complex. *J Biol Chem.* 288:9563-9571.
38. Matti U, Pattu V, Halimani M, Schirra C, Krause E, Liu Y, Weins L, Chang HF, Guzman R, Olausson J, Freichel M, Schmitz F, Pasche M, Becherer U, Bruns D, Rettig J (2013).

Synaptobrevin2 is the v-SNARE required for cytotoxic T-lymphocyte lytic granule fusion. *Nat Commun.* 4:10.1038/ncomms2467.

39. McDonald B, Bunker J, Erickson S, Oh-Hora M, Bendelac A (2015). Crossreactive $\alpha\beta$ T Cell Receptors Are the Predominant Targets of Thymocyte Negative Selection. *Immunity* 43:859-869.
40. McMahon H, Boucrot E (2011). Molecular mechanism and physiological functions of clathrin-mediated endocytosis. *Nature Reviews Molecular Cell Biology* 12:517-533.
41. Medzhitov R, Janeway Jr. CA (1997). Innate immunity: impact on the adaptive immune response. *Current Opinion in Immunology* 9:4-9.
42. Mettlen M, Pucadyil T, Ramachandran R, Schmid S (2010). Dissecting dynamin's role in clathrin-mediated endocytosis. *Biochem Soc Trans.* 37:1022-1026.
43. Nelson B (2004). IL-2, Regulatory T Cells, and Tolerance. *J Immunol* 172:3983-3988.
44. Owen D, Vallis Y, Pearse B, McMahon H, Evans, P (2000). The structure and function of the beta 2-adaptin appendage domain. *EMBO J.* 19:4216-4227.
45. Parkin J, Cohen B (2001). An overview of the immune system. *The Lancet* 357:1778-179.
46. Pattu V, Halimani M, Ming M, Schira C, Hahn U, Bzeih H, Chang HF, Weins L, Krause E, Rettig J (2013). In the crosshairs: investigating lytic granules by high-resolution microscopy and electrophysiology. *Front Immunol.* 4:10.3389/fimmu.2013.00411.
47. Pennuto M, Bonanomi D, Benfenati F, Valtorta F (2003). Synaptophysin I controls the targeting of VAMP2/synaptobrevin II to synaptic vesicles. *Mol Biol Cell.* 12:4909-4919.
48. Peters P, Borst J, Oorschot V, Fukuda M, Krähenühl O, Tschopp J, Slot JW, Geuze HJ (1991). Cytotoxic T Lymphocyte Granules Are Secretory. *J Exp Med.* 173:1099-1109.
49. Rani A, Murphy J (2016). STAT5 in Cancer and Immunity. *J Interferon Cytokine Res.* 36:226-237.
50. Rapoport I, Chen Y, Cupers P, Shoelson S, Kirchhausen T (1998). Dileucine-based sorting signals bind to the beta chain of AP-1 at a site distinct and regulated differently from the tyrosine-based motif-binding site. *EMBO J.* 17:2148-2155.
51. Rizzolo S, Jahn R (2007). Kiss-and-run, collapse and 'readily retrievable' vesicles. *Traffic* 9:1137-44.
52. Smith-Garvin J, Koretzky G, Jordan M (2009). T Cell Activation. *Annual Review of Immunology* 27:591-619.

53. Smyth M, Kelly J, Sutton V, Davis J, Browne K, Sayers T, Trapani JA (2001). Unlocking the secrets of cytotoxic granule proteins. *J Leukoc Biol.* 70:18-29.
54. Stinchcombe J, Bossi G, Booth S, Griffiths G (2001). The immunological synapse of CTL contains a secretory domain and membrane bridges. *Immunity* 15:751-761.
55. Torres A, Contento R, Gordo S, Wucherpfennig K, Love J (2012). Functional single-cell analysis of T-cell activation by supported lipid bilayer-tethered ligands on arrays of nanowells. *Lab Chip.* 13:90-9.
56. Von Gersdorff H, Mathews G (1994). Dynamics of synaptic vesicle fusion and membrane retrieval in synaptic terminals. *Nature* 367:735-739.
57. Watanabe S, Boucrot E (2017). Fast and ultrafast endocytosis. *Current Opinion in Cell Biology* 47:64-71.
58. Watts C (1985). Rapid endocytosis of the transferrin receptor in the absence of bound transferrin. *J Cell Biol.* 100:633-637.
59. Weissler K, Caton A (2014). The role of T-cell receptor recognition of peptide:MHC complexes in the formation and activity of Foxp3⁺ regulatory T cells. *Immunol Rev.* 259:11-22.
60. Wiedeman A, Depoil D, Faroudi M, Valitutti S (2006). Cytotoxic T lymphocytes kill multiple targets simultaneously via spatiotemporal uncoupling of lytic and stimulatory synapses. *Proc Natl Acad Sci U S A.* 109:10985-90.
61. Wolint P, Betts M, Koup R, Oxenius A (2004). Immediate cytotoxicity but not degranulation distinguishes effector and memory subsets of CD8⁺ T cells. *J Exp Med.* 199:925-36.
62. Wu M, Huang B, Graham M, Raimondi A, Heuser J, Zhuang X, De Camilli P (2010). Coupling between clathrin-dependent endocytic budding and F-BAR-dependent tubulation in a cell-free system. *Nat Cell Biol.* 12:902-908.
63. Xie Z, Long J, Liu J, Chai Z, Kang X, Wang C (2017). Molecular Mechanisms for the Coupling of Endocytosis to Exocytosis in Neurons. *Front Mol Neurosci.* 47:10-17.
64. Yatim K, Lakkis F (2015). A Brief Journey through the Immune System. *Clin J Am Soc Nephrol.* 10:1274-1281.

10 ACKNOWLEDGEMENTS

I want to thank all the people who helped me accomplishing my research and enabling me to complete this thesis. First of all, I would like to express my deepest gratitude to my supervisor Prof. Dr. Jens Rettig for his support, his brilliant ideas and his guidance over the past months and years. He did not only promote my ideas and scientific progress but also much supported my medical career and personal development. I am very thankful to have met him as my mentor.

Furthermore, I would like to thank my principal investigator, Dr. Varsha Pattu, for always taking care of any problems and giving great support in any situation. I also appreciate the support of Priv.-Doz. Dr. Ute Becherer regarding the TIRF setup and her excellent help in any problematic imaging analysis. I would like to thank Priv.-Doz. Dr. Elmar Krause, Dr. Davis Stevens, and Dr. Claudia Schirra for always having an open door for me. I want to express my many thanks to Margarete Klose who was the best help in producing the lipid bilayer. I also thank the technicians Tamara Paul, Anja Ludes, and Katrin Sandmeier for exceptional technical support. I enjoyed working together with the most enjoyable colleagues and friends Praneeth Chitirala, Marwa Sleiman, Keerthana Ravichandran, Angelina Staudt, Olga Ratai and Priya Katiyar.

Finally, my many thanks to my family, especially to my uncle Dr. Achim Blatt, who is an excellent support in all respects and a very skillful proofreader.

Datum der mündlichen Prüfung: 26.02.2020

Dekan: Prof. Dr. Michael Menger

Erstberichterstatter: Prof. Dr. Jens Rettig

Zweitberichterstatter: Prof. Dr. Markus Hoth